



**HAL**  
open science

# Seasonal variations of the physical and optical characteristics of Saharan dust: Results from the Dust Outflow and Deposition to the Ocean (DODO) experiment

C. McConnell, E. Highwood, H. Coe, P. Formenti, B. Anderson, S. Osborne, S. Nava, K. Desboeufs, G. Chen, M. Harrison

## ► To cite this version:

C. McConnell, E. Highwood, H. Coe, P. Formenti, B. Anderson, et al.. Seasonal variations of the physical and optical characteristics of Saharan dust: Results from the Dust Outflow and Deposition to the Ocean (DODO) experiment. *Journal of Geophysical Research: Atmospheres*, 2008, 113 (D14), 10.1029/2007JD009606 . hal-04254149

**HAL Id: hal-04254149**

**<https://hal.science/hal-04254149>**

Submitted on 24 Oct 2023

**HAL** is a multi-disciplinary open access archive for the deposit and dissemination of scientific research documents, whether they are published or not. The documents may come from teaching and research institutions in France or abroad, or from public or private research centers.

L'archive ouverte pluridisciplinaire **HAL**, est destinée au dépôt et à la diffusion de documents scientifiques de niveau recherche, publiés ou non, émanant des établissements d'enseignement et de recherche français ou étrangers, des laboratoires publics ou privés.

Copyright

## Seasonal variations of the physical and optical characteristics of Saharan dust: Results from the Dust Outflow and Deposition to the Ocean (DODO) experiment

C. L. McConnell,<sup>1</sup> E. J. Highwood,<sup>1</sup> H. Coe,<sup>2</sup> P. Formenti,<sup>3</sup> B. Anderson,<sup>4</sup> S. Osborne,<sup>5</sup> S. Nava,<sup>6</sup> K. Desboeufs,<sup>3</sup> G. Chen,<sup>4</sup> and M. A. J. Harrison<sup>5</sup>

Received 15 November 2007; revised 20 March 2008; accepted 24 April 2008; published 28 June 2008.

[1] North African dust is important for climate through its direct radiative effect on solar and terrestrial radiation and its role in the biogeochemical system. The Dust Outflow and Deposition to the Ocean project (DODO) aimed to characterize the physical and optical properties of airborne North African dust in two seasons and to use these observations to constrain model simulations, with the ultimate aim of being able to quantify the deposition of iron to the North Atlantic Ocean. The in situ properties of dust from airborne campaigns measured during February and August 2006, based at Dakar, Senegal, are presented here. Average values of the single scattering albedo (0.99, 0.98), mass specific extinction ( $0.85 \text{ m}^2 \text{ g}^{-1}$ ,  $1.14 \text{ m}^2 \text{ g}^{-1}$ ), asymmetry parameter (0.68, 0.68), and refractive index ( $1.53-0.0005i$ ,  $1.53-0.0014i$ ) for the accumulation mode were found to differ by varying degrees between the dry and wet season, respectively. It is hypothesized that these differences are due to different source regions and transport processes which also differ between the DODO campaigns. Elemental ratios of Ca/Al were found to differ between the dry and wet season (1.1 and 0.5, respectively). Differences in vertical profiles are found between seasons and between land and ocean locations and reflect the different dynamics of the seasons. Using measurements of the coarse mode size distribution and illustrative Mie calculations, the optical properties are found to be very sensitive to the presence and amount of coarse mode of mineral dust, and the importance of accurate measurements of the coarse mode of dust is highlighted.

**Citation:** McConnell, C. L., E. J. Highwood, H. Coe, P. Formenti, B. Anderson, S. Osborne, S. Nava, K. Desboeufs, G. Chen, and M. A. J. Harrison (2008), Seasonal variations of the physical and optical characteristics of Saharan dust: Results from the Dust Outflow and Deposition to the Ocean (DODO) experiment, *J. Geophys. Res.*, *113*, D14S05, doi:10.1029/2007JD009606.

### 1. Introduction

[2] Mineral dust is an important species in the Earth's atmosphere. Picked up from the surface around the globe, the majority of this dust is a natural aerosol although models suggest that 5–7% of the global dust loading is anthropogenic in origin [Teegen *et al.*, 2004] and this may be between 0 and 15% in the North African region [Yoshioka *et al.*, 2005]. Activities such as land use change and overgrazing increase the dust available for uplift [e.g., Teegen and Fung, 1995]. Dust is lifted from land surfaces across the globe, but Saharan mineral dust accounts for an annual source of 400–700 Tg a<sup>-1</sup> [Washington *et al.*, 2003], a large proportion of the total. Dust is emitted from sources within North Africa,

of which the Sahara forms the major part [e.g., Woodward, 2001], and can be advected across the Atlantic toward the southeast USA and South America [Prospero, 1999; Formenti *et al.*, 2001; Reid *et al.*, 2003]. Some of this dust advection occurs during Africa-wide outbreaks [e.g., Slingo *et al.*, 2006]; there has been somewhat less focus on the properties of airborne dust during less extreme outbreaks and throughout the year.

[3] The most direct way in which mineral dust can influence global climate is by scattering and absorbing radiation, affecting both regional and global energy balance. Mineral dust, perhaps most interestingly of all aerosols, can affect both solar and terrestrial radiation. In the shortwave part of the spectrum, dust scatters radiation back to space but depending on the albedo of the underlying surface it can either increase (over ocean) or make little difference (over desert) to the total albedo. The impact in the longwave depends crucially on the surface temperature and the altitude of the dust layer. Radiation from the ground is absorbed in the dust layer and reemitted back toward the ground thereby potentially increasing the surface temperature. For dust over the ocean surface the result is usually dominated by the solar effect, however for dust at altitude

<sup>1</sup>Department of Meteorology, University of Reading, Reading, UK.

<sup>2</sup>School of Earth, Atmosphere and Environmental Science, University of Manchester, Manchester, UK.

<sup>3</sup>LISA, CNRS, Universités Paris 12 et Paris 7, Créteil, France.

<sup>4</sup>NASA Langley Research Center, Hampton, Virginia, USA.

<sup>5</sup>Met Office, Exeter, UK.

<sup>6</sup>National Institute of Nuclear Physics, Florence, Italy.

over a desert surface the longwave effect can dominate the flux changes at the top of the atmosphere. It is also important to distinguish between the effect at the top of the atmosphere and at the surface, since the direct solar radiation reaching the ground can be dramatically reduced while the diffuse component increases substantially during major dust outbreaks. The impact of dust on longwave radiation is important for satellite retrievals of sea surface temperature and the spectral signal within the 8–12  $\mu\text{m}$  region can be used to infer the mineralogy of the dust [Highwood *et al.*, 2003]. The Saharan Dust Experiment (SHADE) surveyed the optical properties and radiative impact of Saharan dust during September 2000 [Haywood *et al.*, 2003]. Magnitudes for the local direct radiative effect over the ocean reached as much as  $-130 \text{ W m}^{-2}$  at the top of the atmosphere for an individual dust storm. Slingo *et al.* [2006] also showed top of atmosphere shortwave flux increased by  $100 \text{ W m}^{-2}$  while the surface downward solar flux at Niamey reduced by as much as  $300 \text{ W m}^{-2}$  for the dust storm of early March 2006. These are considerable perturbations to the local energy balance. In terms of global climate change, the IPCC 2007 report considered the anthropogenic dust top of the atmosphere radiative forcing to range between  $-0.3 \text{ W m}^{-2}$  and  $+0.1 \text{ W m}^{-2}$  [Forster *et al.*, 2007]. Key parameters for determining the radiative effect of dust include the single scattering albedo ( $\omega_0$ ), the asymmetry parameter ( $g$ ), and the mass specific extinction ( $k_{\text{ext}}$ ), which are dependent on size distribution and refractive index.

[4] Other impacts of North African dust on the climate system are less well studied and quantified. Even small concentrations of mineral dust are thought to be able to significantly affect cold cloud properties including the radiative properties of cirrus, dehydration of the tropopause and convective cloud dynamics. Laboratory studies show that dust might act as ice nuclei and have shown dust to exhibit complex primary and secondary nucleation at varying ice supersaturations [e.g., Field *et al.*, 2006]. Accordingly, DeMott *et al.* [2003] results from CRYSTAL-FACE (The Cirrus Regional Study of Tropical Anvils and Cirrus Layers–Florida Area Cirrus Experiment) showed that Saharan dust plumes were associated with elevated ice nuclei counts across Florida, while Richardson *et al.* [2007] showed a proportionately high contribution to ice nuclei by mineral dust over the continental USA. It has also been hypothesized that dust may provide a surface for heterogeneous chemical reactions to take place. For example, ozone can be destroyed on pure calcium carbonate particles. Salisbury *et al.* [2006] found that daily cycles and absolute concentrations of some oxygenated species were different during dust storms in the MINATROC (Mineral dust aerosol and tropospheric chemistry) project. However, it was impossible to unequivocally attribute this to heterogeneous reactions on the dust itself.

[5] Airborne North African dust is of great interest to marine biologists. Much of the dust leaving the western coast of Africa is deposited in the Atlantic Ocean where it provides a flux of nutrients such as iron and phosphorus to the ocean. This deposition stimulates nitrogen fixation and relieves iron limitation of phytoplankton activity. The resulting growth of marine biological organisms results in ocean sequestration of carbon dioxide and fluxes of hal-

ocarbons, alkylnitrate and DMS between atmosphere and ocean. Iron from mineral dust therefore plays an indirect route in carbon and other mass fluxes between atmosphere and ocean [Jickells *et al.*, 2005].

[6] One climate impact which has received much interest in recent years has been the role of North African dust in tropical storm and hurricane formation. Jones *et al.* [2004] reported indirect observations of modification of African Easterly Waves (the forerunner disturbances of some hurricanes) via the radiative impacts of dust. Evan *et al.* [2006] showed that mean dust coverage as measured by satellites and tropical cyclone activity are strongly correlated over the North Atlantic. Particular highlight has been given to the contrasting North Atlantic hurricane seasons of 2005 (active, fewer dust outbreaks than normal) and 2006 (less active, more dust outbreaks than normal). However, this is not in itself enough to suggest that the dust is directly influencing the tropical cyclones. Various mechanisms including the radiative impact on sea surface temperature, and alteration of vertical shear regions, and the entrainment of dust laden dry air have been proposed. However, none of these have been shown to be a predominant governor of cyclone activity, with N. Atlantic sea surface temperatures playing a very large role in determining the cyclone activity. The correlation between dust and cyclone activity may stem from them both being driven by a third party, for example Sahelian rainfall in the previous season.

[7] Because of the significant destructive capacity of hurricanes, there is considerable interest in summer season dust uplift and transport. The mechanisms of dust production and uplift are rather different between dry season (November to March) and the wet season (July–September). During the dry season, dust in western Africa is mainly found at low altitudes and its uplift often results from activity along trailing cold fronts associated with systems passing through the Mediterranean region. Orography and local advection effects then magnify the dust uplift [e.g., Slingo *et al.*, 2006]. The winter season, therefore, tends to produce very dramatic dust outbreaks that last a few days. During the wet season, dust tends to be uplifted in convection over the African continent and then transported westward at altitude. The different transport mechanisms between seasons could have an effect on the size distribution of dust, and hence result in different optical properties. The vertical profiles of dust also vary substantially between seasons [e.g., Karyampudi *et al.*, 1999; Zhu *et al.*, 2007], which will also have an impact on the radiative effect.

[8] In addition, there is evidence that the African source regions may differ throughout the year [e.g., Schepanski *et al.*, 2007; Washington *et al.*, 2003; Chiapello *et al.*, 1997]. The Bodélé Depression in Chad is perhaps the major source region for mineral dust, but there are significant sources in the western Sahara which also influence the dust flowing toward the Atlantic. As shown by Washington and Todd [2005] and Engelstaedter and Washington [2007], there is evidence that the uplift from these different sources responds to different parts of the atmospheric dynamics. In the case of the Bodélé Depression the presence and strength of the low-level jet is important, while dust production from the western Sahara seems to be more closely related to the degree of low-level convergence. Differing mineralogy at these sources may influence the

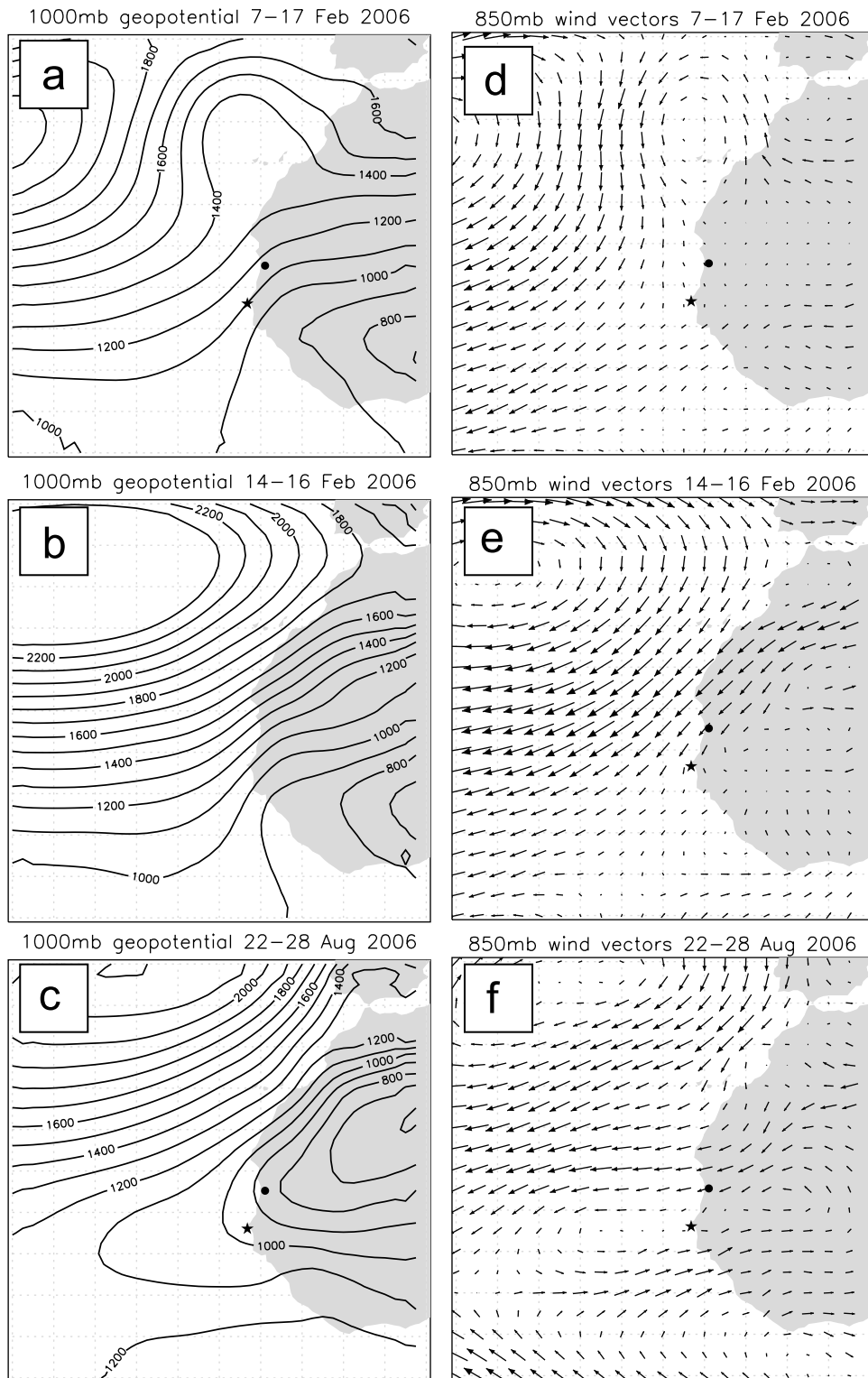


**Figure 1.** DODO campaign meteorology from ERA operational analyses. The 1000 mbar geopotential ( $m^2 s^{-1}$ ) for (a) DODO1 period 7–17 February 2006, (b) DODO1 period 14–16 February 2006, and (c) DODO2 period 22–28 August 2006. The 850 mbar wind vectors for (d) DODO1 period 7–17 February 2006, (e) DODO1 period 14–16 February 2006, and (e) DODO2 period 22–28 August 2006. Locations of Dakar and Nouakchott are indicated by a star and circle, respectively.

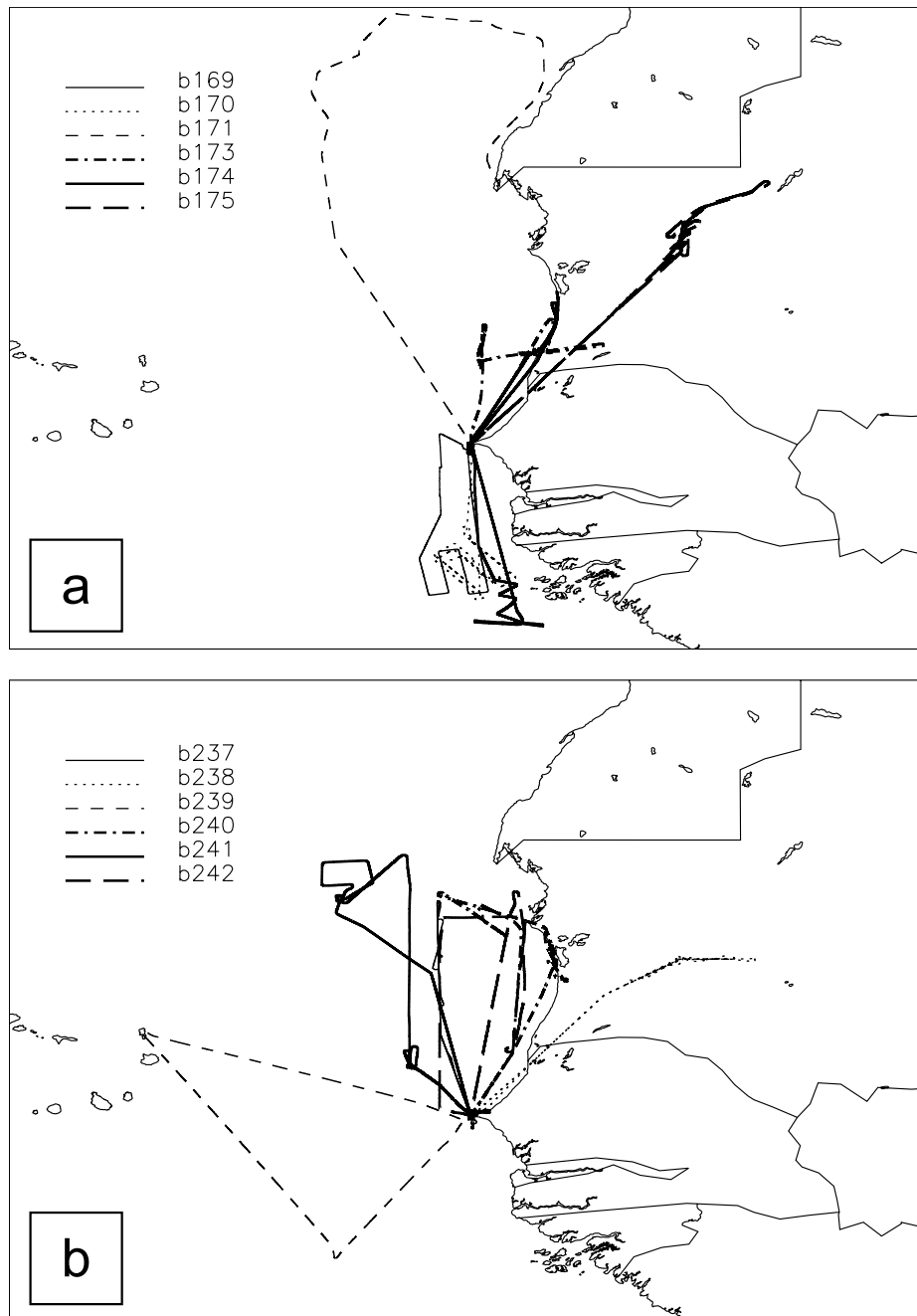


**Figure 2.** Flight tracks for (a) DODO1 and (b) DODO2 campaigns based in Dakar, Senegal.

composition of mineral dust [Claquin *et al.*, 1999; Formenti *et al.*, 2008] and its microphysics, and thus the radiative impact [e.g., Todd *et al.*, 2007; Highwood *et al.*, 2003].

[9] It is important to remember that dust is not the only aerosol that affects sub Saharan Africa. During the dry season, considerable biomass burning activity along the coast of the Gulf of Guinea and convection there results in a ubiquitous layer of biomass burning aerosol at higher altitudes above the dust, and this complicates retrieval of aerosol properties from AERONET (Aerosol Robotic Network) and satellite methods as biomass burning aerosol has quite different properties to dust. The interaction of dust and

biomass during January–February 2006 was examined in detail by the Dust and Biomass Experiment (DABEX) of the UK Met Office [Johnson *et al.*, 2008; J. M. Haywood *et al.*, Overview of the Dust and Biomass Burning Experiment and African Monsoon Multidisciplinary Analysis Special Observing Period-0, submitted to *Journal of Geophysical Research*, 2008] and parallels between dust and biomass found during that campaign and those reported here are discussed by Osborne *et al.* [2008].

[10] In terms of understanding the climate impact of dust throughout the year there is clearly a need to establish whether the likely seasonal differences in uplift and trans-

**Table 1.** Summary of Flights During DODO1 and DODO2 Campaigns

Flight Number	Date	Takeoff, Landing	Operating Area	Objectives
DODO1				
B169	7 Feb 2006	112228, 141834	over ocean south of Dakar	instrument shake-down, biomass burning aerosol sampling
B170	11 Feb 2006	095447, 145335	over ocean south of Dakar	in situ biomass aerosol collection
B171 (B172)	12 Feb 2006	084911, 130656	north of Nouadhibou, over ocean	model validation for major dust storm to north of region; aircraft lost science power during refuel therefore no data available from B172
B173	14 Feb 2006	094953, 143615	coastal region, Dakar-Nouackchott	in situ sampling of local dust source
B174	15 Feb 2006	094400, 131354	over sea north and south of Dakar	in situ sampling of dust advected over ocean and biomass aerosol
B175	16 Feb 2006	085143, 141538	land regions in northern Mauritania	in situ sampling and radiometric measurements over land, moderate dust loading
DODO2				
B237	22 Aug 2006	135855, 182401	over ocean northwest of Dakar	in situ and radiation measurements of dust over ocean off Senegal/Mauritania coast
B238	23 Aug 2006	130025, 173152	land regions in northern Mauritania	sample heavy dust loadings over land in Mauritania forecast by dust models and visible in satellite imagery
B239	24 Aug 2006	095141, 135328	over ocean, between and to the south of Dakar and Sal	in situ measurements of dust forecast over ocean to south of Dakar-Sal area
B240	24 Aug 2006	151619, 193645	over ocean northwest of Dakar	mapping of in situ dust to north of Dakar for comparison with B239
B241	25 Aug 2006	135438, 183200	over ocean between Nouadhibou and Dakar	intercomparison flight with NASA DC8 and high-level calibration of radiometers
B242	28 Aug 2006	110243, 153338	over ocean northwest of Dakar	in situ and radiation measurements of moderate dust loadings to north of Dakar

port processes lead to any discernible influence in radiative or microphysical properties. From a biogeochemical point of view, these may also lead to differences in nutrient deposition to the ocean. The Dust Outflow and Deposition to the Ocean (DODO) project was conceived to use aircraft measurements of airborne dust to constrain model estimates of dust deposition to the ocean. The microphysical and optical properties and the vertical structure the dust that were measured during the two major fieldwork periods in Africa are described in this paper. Section 2 describes the airborne campaigns and instrumentation in more detail, including measurement correction procedures based on an intercomparison flight with the NASA DC-8 aircraft. The characteristics of dust found during both DODO campaigns are described in sections 3, 4 and 5. The paper ends with discussion in section 6. The project is ongoing, and model results will be reported elsewhere in due course.

## 2. Methodology

### 2.1. DODO Meteorology and Flight Patterns

[11] In order to characterize airborne North African dust and outflow to the ocean in both the dry season and the wet season, two airborne campaigns based in Dakar, Senegal, were organized. DODO1 took place during the dry season from 7 to 16 February 2006, while DODO2 followed in the wet season from 22 to 28 August. Both campaigns were also associated with the AMMA (African Monsoon Multi-disciplinary Analysis) project [Redelsperger *et al.*, 2006]. The 1000 mbar geopotential and 850 mbar wind vectors are shown in Figure 1, for the whole of DODO1 (Figures 1a and 1d), the last 3 days of DODO1 (Figures 1b and 1e), and the whole of DODO2 (Figures 1c and 1f). During DODO1 the flow changed substantially: for the first week the flow was dominated by an anomalous low-pressure system

located over the Canary Islands, shown by the geopotential lines in Figure 1a, which resulted in little offshore flow in the region between Dakar and Nouakchott (Figure 1d). This is contrary to the predominantly easterly flow that would be expected from climatology [e.g., Hastenrath, 1991] and no dust was sampled during this period. The flow changed during the three final days of the campaign, becoming more climatological with northerly/northeasterly flow to the north of Dakar (Figures 1b and 1e), advecting light dust loadings toward Dakar. During this period the dust samples discussed in this study were collected on flights B173, B174 and B175 (Figure 2a). This flow pattern is not reflected in the DODO1 averages (Figures 1a and 1d) because of its short time duration. To the south of Dakar the flow was offshore (see Figure 1d) giving rise to the advection of biomass aerosol (originating from southern West Africa) at midlevels in the troposphere, this being sampled during three of the six DODO1 flights which operated to the south of Dakar (see Figure 2a).

[12] The geopotential in Figure 1c shows the Saharan heat low positioned over Algeria during DODO2. The wind vectors at 850 mbar suggest offshore flow to the north of Dakar, with a recirculation to the south of the region. However, it is important to note that these mean circulation patterns are a combination of flow patterns from a succession of African easterly waves that passed over Dakar during this time, bringing relatively large meridional excursions of alternately dry and moist airflow over Dakar. The six flights during DODO2 concentrated mainly on the ocean and land areas to the north of Dakar (Figure 2b), reflecting the largest likelihood of dust sampling. During DODO2, Dakar itself was frequently affected by clouds associated with Mesoscale Convective Systems which passed mainly to the south of the main operating area. A summary of the

**Table 2.** Summary of Aerosol-Related Instruments on Board the FAAM BAe146 Operated During the DODO Campaigns

Type of Measurement	Instrument	Size Range (Optically Equivalent Radius), Wavelengths, etc.	Comment
Aerosol microphysics	PMS PCASP, GRIMM OPC, DMT CDP	0.05–1.5 $\mu\text{m}$ , 0.15–20 $\mu\text{m}$ , 2.5–20 $\mu\text{m}$	
Aerosol optical properties	TSI nephelometer, PSAP	$\lambda = 0.45, 0.55, 0.7 \mu\text{m}$ ; $\lambda = 0.567 \mu\text{m}$	particle scattering coefficient, particle absorption coefficient
Aerosol chemical composition	bulk filters, Aerodyne AMS, VACC	90-mm Nuclepore 0.4 $\mu\text{m}$ pore size; quartz; Particle sizes 50–500 nm; temperature range 50–300°C, PCASP 0.05–1.5 $\mu\text{m}$	inorganics (elements and water soluble fraction), carbon (EC and OC), volatile and semivolatile aerosols, water and volatile material
Trace gas chemistry	O <sub>3</sub> , CO		O <sub>3</sub> and CO are sampled using online analyzers
Thermodynamics	AVAPS		temperature, pressure, winds, GPS

location, duration and nature of the flights in both DODO campaigns is given in Table 1.

[13] In this study results are presented for aircraft maneuvers consisting of vertical profiles, measuring the vertical distribution of aerosol, and straight and level runs, measuring in situ aerosol for a duration of between 5 and 30 min at a constant altitude. Vertical profiles range from either ground level (in the case of takeoff or landing) or the aircraft's minimum safe altitude of 50ft over sea or approximately 500ft over land, to above the aerosol layer. The aircraft flies at 110 m s<sup>-1</sup> but ascends/descends at 5 m s<sup>-1</sup> and therefore covers considerable horizontal distance during a profile, which means that the straight and level run data is valuable in terms of showing the horizontal variation. Most instruments on the BAe146 (including the nephelometer) sample at least 1Hz, giving good resolution of data in the vertical and horizontal. Straight and level runs will hereafter be referred to as "runs."

## 2.2. BAe146 Instrumentation

[14] The core instrumentation on the UK community Facility for Airborne Atmospheric Measurements (FAAM) BAe146 is described by Haywood et al. (submitted manuscript, 2008). Details of the most relevant instrumentation for aerosol and dust measurements are given in Table 2. Key instruments included the wing-mounted Passive Cavity Aerosol Spectrometer Probe (PCASP), TSI integrating nephelometer model 3563 and Radiance Research Particle Soot Absorption Photometer (PSAP) (corrected according to standard procedures as in the work by Bond et al. [1999]) in terms of aerosol microphysical and optical properties for the accumulation mode.

[15] Bulk filters were used to collect samples of airborne dust. The aerosol sampling system used on board the BAe146 is identical to that previously used on board the UK Met Office C-130 and is described in detail by Andreae et al. [2000], who estimated the inlets to the filters to sample 35% of the coarse mode by mass. Aerosol particles were sampled by filtration onto two stacked filter units (SFUs) mounted in parallel. Each SFU can hold a maximum of three filters on sequential 47-mm diameter polyethylene supports, but only one stage was used during DODO. Samples were collected only during horizontal flight legs lasting not less than 20–30 min in order to guarantee sufficient loading of the filter samples. One SFU consisted of a Nucleopore filter (nominal pore size 0.4  $\mu\text{m}$ ) measuring the inorganic composition. The second SFU was used for measuring carbonaceous aerosols on one quartz filter.

### 2.2.1. Nephelometer Corrections Using the DC-8 Intercomparison

[16] During DODO2, the BAe146 flew a wing tip to wing tip comparison flight (B241) with the NASA DC-8. Flight B241 included 3 straight and level runs within the Saharan Air Layer over the Atlantic Ocean to the north of the Cape Verde Islands (see Figure 2b). This provided an opportunity to compare the nephelometers on board both aircraft. The BAe146 was operating a TSI 3563 nephelometer running from a Rosemount inlet, which has been estimated by Haywood et al. [2003] to have an upper limit for dust particles at around 3  $\mu\text{m}$  in terms of optical diameter, although the true cutoff is not well defined. The DC-8 operated a TSI 3563 nephelometer behind the NASA LaRC type inlet. This inlet has been shown to give a 50% loss of dust particles above 3.6  $\mu\text{m}$  aerodynamic diameter (giving an optically equivalent diameter of 2.0  $\mu\text{m}$  [McNaughton et al., 2007]).

[17] Figure 3 shows the scattering from the DC-8 and the BAe146 TSI nephelometers during one of the three straight and level runs from flight B241. In each case, both nephelometers measured dry scattering at low values of relative humidity and the data has been corrected as advised by Anderson and Ogren [1998]. Relative humidity during these runs varied between 52% to 69% and so no attempt

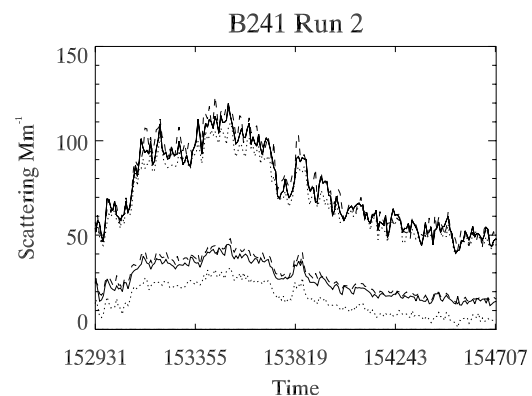


**Figure 3.** Nephelometer measurements of scattering in  $\text{Mm}^{-1}$  from intercomparison flight B241 (BAe146 run 2) at 2100 m within dust layer. Heavy lines are BAe146 measurements corrected according to Anderson and Ogren [1998]. Light lines are DC-8 TSI nephelometer data corrected similarly. Dotted lines are 450 nm, solid lines are 550 nm, and dashed lines are 700 nm.

**Table 3.** Linear Pearson Correlation Coefficients ( $r$ ) Between DC-8 and BAe146 Data During Three Wing Tip to Wing Tip Straight and Level Runs Within Dust Layers During DODO2 Flight B241

Channel	Run 1	Run 2	Run 3
0.45 $\mu\text{m}$	0.93	0.96	0.93
0.55 $\mu\text{m}$	0.82	0.97	0.94
0.70 $\mu\text{m}$	0.80	0.94	0.91

has been made to account for any hygroscopic growth, which is thought to be small for dust particles within this range of humidities [e.g., *Li-Jones et al.*, 1998; *Carrico et al.*, 2003] It is apparent that the two nephelometers are sampling similar variability in the aerosol layer (i.e., spatial variability) however there is a significant offset between the two instruments, with the BAe146 scattering being substantially lower than the DC-8. In addition, the 450 nm channel on the BAe146 nephelometer is reading relatively much lower than other frequencies compared to the DC-8. The ratio between DC-8 and BAe146 values is approximately 2.5 in each of the 3 runs. Table 3 shows the linear Pearson correlation coefficients ( $r$ ) for scattering measured by the two systems at the three different wavelengths during the three different straight and level runs within dust. The average ratios of the DC-8 to BAe146 scattering across the three runs were 7.3, 2.36 and 2.4 at 450, 550 and 700 nm respectively.

[18] The combined evidence of (1) high correlation between the two nephelometers at all wavelengths and in all three runs, (2) higher scattering measured by the DC-8 nephelometer by a factor of 2.5, and (3) underestimation of aerosol optical depth by the nephelometer and PSAP compared to AERONET by an average factor of 3.1 (see following paragraph), point to a fault with the BAe146 nephelometer, suggesting a sensitivity loss perhaps due to the high dust loadings experienced during an immediately preceding campaign where the nephelometer was not closely monitored and which may have resulted in the detectors becoming dirty. On the basis of the similar inlet cutoff diameters on the two aircraft and the large differences in scattering between the two nephelometers, it is thought unlikely that the differences in scattering are due to the DC-8 inlet having a greater passing efficiency.

[19] It was therefore decided that for DODO2, the BAe146 nephelometer data would be scaled to agree with the DC-8 TSI data. A linear fit was used to fit the BAe146 data to the DC-8 data. The resulting corrections using the average fit parameters across all three runs for 450, 550 and 700  $\mu\text{m}$  channels of the BAe146 scattering data are shown below.

$$\sigma_{corr}^{450} (\text{in m}^{-1}) = 33.2 \times 10^{-6} + 7.3 \times \sigma^{450} \quad (1)$$

$$\sigma_{corr}^{550} (\text{in m}^{-1}) = 11.3 \times 10^{-6} + 2.36 \times \sigma^{550} \quad (2)$$

$$\sigma_{corr}^{700} (\text{in m}^{-1}) = 10.1 \times 10^{-6} + 2.4 \times \sigma^{700} \quad (3)$$

Note that a larger correction for blue wavelengths is required because of the very low scattering at blue

wavelengths compared to red and green wavelengths. Figure 4 shows the effect of this correction for one of the straight and level runs, the triangles representing the correlation of the original BAe146 data with the DC-8 data, and the diamonds the improved correspondence when the fits in equations (1)–(3) above are applied. It should be noted that the uncertainty in passing efficiency of the BAe146 Rosemount inlet relative to the DC-8 LaRC type inlet results in a small amount of uncertainty in applying the scaling factor from the intercomparison flight B241 to the other DODO2 flights where the aerosol size distributions and optical properties may be different.

[20] The underestimation of scattering by the BAe146 nephelometer can also be shown by comparing optical depths measured by the Dakar AERONET station at Mbour to those obtained by integrating the vertical profiles of scattering in the vicinity of the only AERONET station, according to the expression:

$$\tau_{550} = \int_0^z \frac{\sigma_{corr}^{550}}{\omega_0^{550}} dz \quad (4)$$

where  $\omega_0^{550}$  is the single scattering albedo calculated from a horizontal run in a dust layer at an appropriate altitude. PSAP data is only used for straight and level runs when the flow rate has been manually set to 3 L per minute and integration of absorption measured by the PSAP during profiles is not possible as the flow rate is not recorded on the BAe146. The comparison of calculated AODs with those measured by AERONET is shown in Table 4. DODO1 profiles (assumed to be unaffected by the nephelometer issues, but still affected by any inlet losses) underestimate AOD compared to AERONET by a factor of 1.54 which is consistent with previous experience during SHADE [*Haywood et al.*, 2003], this being attributed to loss of coarse mode particles in the instrument inlet. The DODO2 comparison using data corrected using the DC-8

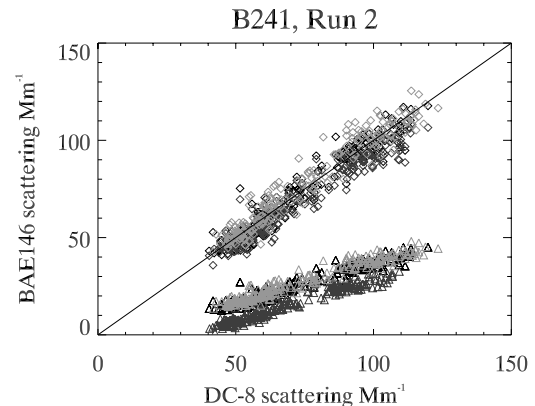


**Figure 4.** Correlation plot of DC-8 and BAe146 nephelometer measurements from BAe146 runs 1–3 of flight B241. Triangles show BAe146 data with correction only according to *Anderson and Ogren* [1998]. Diamonds show BAe146 data corrected according to a linear fit against the DC-8 data at each of three wavelengths and averaged across all three runs. Heaviest symbols are 550 nm, and palest are 700 nm.

**Table 4.** Correction Factors Obtained From Comparing AERONET Optical Depths at Dakar With Integrated Extinction From Accumulation Mode Measurements During Aircraft Profiles at Dakar

Flight	Profile	Aircraft-Based Optical Depth $\tau^{550}$	AERONET Optical Depth at 550 nm $\tau_{\text{AERONET}}$	$C = \tau_{\text{AERONET}}/\tau^{550}$
DODO1				
B168	P17	0.21	0.38	1.83
B169	P1	0.30	0.24	0.81
B171	P1	0.11	0.11	1.00
B173	P1	0.09	0.12	1.34
B174	P10	0.05	0.11	2.03
B175	P1	0.12	0.15	1.19
B175	P8	0.04	0.11	2.56
Mean				1.54
DODO2				
B236	P10	0.33	0.23	0.71
B237	P8	0.61	0.64	1.06
B238	P1	0.38	0.68	1.80
B238	P9	0.42	0.48	1.16
B242	P1	0.18	0.42	2.30
B242	P11/P12	0.27	0.29	1.08
Mean				1.35

data gives a similar underestimate, whereas using data not corrected in equation (2) the aerosol optical depth was underestimated by a factor of 3.1.

[21] The variability of the underestimation of aerosol optical depth shown in Table 4 is assumed to be related to differing amounts of coarse mode aerosol being present, although some of the variation may be explained by discrepancies in inlet passing efficiency between the two aircraft which would result in a different scaling factor being required for different size distributions. As concerns hygroscopic growth, few estimates of hygroscopicity of Saharan dust exist, but it is likely that relative humidity effects are small. When dust is mixed with large amounts of other aerosols, humidity can be more important, but using the hygroscopic growth values for submicron Asian dust mixtures of Carrico *et al.* [2003] and biomass burning aerosol hygroscopic growth characteristics from Magi and Hobbs [2003] with our profiles resulted in AOD estimates far larger than those from AERONET. Therefore we do not account for hygroscopic growth here, but acknowledge that this could result in small increases in the calculation of AOD. The average distance between the mean profile location and the AERONET station varies between 29 and 254 km (mean of 114 km). Despite some of the profiles being further away from the AERONET station there is no correlation between distance to the AERONET station and the ratios of the AODs, so this is unlikely to be the main cause of differences in AOD.

[22] The comparison of AERONET and aircraft-measured AODs points to a consistency between approaches and supports that the scaling of the BAe146 nephelometer to the DC-8 nephelometer. Further examination, on a flight by flight basis, of the nephelometer behavior during the AMMA airborne campaign immediately prior to the DODO2 campaign suggests that the instrument apparently developed a problem just before deployment in DODO2, a problem that we were not able to rectify in the field. Unfortunately it is not possible from these comparisons to ascertain precisely the problem with the BAe146 nephelometer during DODO2, although loss in the inlets of larger particles is certainly a contributing factor, and this is partly

responsible for the underestimation of AOD in both DODO campaigns. No further attempts were made to adjust the nephelometer scattering data for hygroscopic growth for the cases presented here, based on low relative humidity values during runs sampling dust (46% on average during the whole of DODO) and low expected hygroscopic growth rates for dust particles [e.g., Li-Jones *et al.*, 1998; Carrico *et al.*, 2003].

### 2.2.2. Measurement of Size Distribution

[23] The accumulation mode is measured by a wing-mounted PCASP which measures particles sized between 0.05 and 1.5  $\mu\text{m}$  optically equivalent radius. It is assumed to sample at 100% efficiency at all sizes because of the short sampling lines and relatively small maximum size. Errors in the PCASP-measured size distribution due to nonspherical particles [Osborne *et al.*, 2008] are moderate compared to other sources of uncertainty affecting the optical properties presented here.

[24] Measurements of the coarse mode size distribution are much less well defined than those for the accumulation mode [e.g., Reid *et al.*, 2003], and measurement techniques on the FAAM BAe146 are less well validated. During DODO2 the coarse mode was measured by a Droplet Measurement Technology cloud droplet probe (CDP-100) (see Table 2) and by particle counting software used on scanning electron microscope (SEM) analysis images from filter samples (see Table 2). An internal optical probe was run but line losses prevented any meaningful numbers being used for the supermicron sizes. Limitations of each technique for measuring the coarse mode and the processing of the size distributions in order to allow comparisons are as follows:

[25] 1. The CDP is mounted nonoptimally 10 cm away from the aircraft skin which resulted in some initial uncertainty in the sample volume as a function of particle size [Abel, 2007]. Subsequent comparisons with several cloud instruments, including FSSP-100, Johnson-Williams, Small Ice Detector and Nevzorov were used to determine the sample volume which showed a consistent behavior for droplet sizes below 20  $\mu\text{m}$  radius [Abel, 2007]. On the basis of these comparisons the CDP number concentration for

particles up to a radius of 20  $\mu\text{m}$  has been adjusted by a factor of 0.35 to account for uncertainties in the sample volume. Above 20  $\mu\text{m}$  radius the CDP has a shadowing effect due to its position on the aircraft and hence data from sizes larger than this has been discounted. The lower edge of the smallest CDP size bin is not well characterized and has also been discounted. To create a full size distribution the CDP size distribution has simply been joined onto the PCASP size distribution, and in most cases the transition from PCASP to CDP size distribution appears smooth.

[26] 2. Filter samples were also used to obtain another estimate of the coarse mode size distribution. SEM analysis was performed at the Laboratoire Interuniversitaire des Systèmes Atmosphériques (LISA) in Créteil, France. Particle counting software was used on SEM images of dust samples to obtain a size distribution (as described by *Chou et al.* [2008]). The smallest 4 size bins from the SEM size distribution were defined to be the same as the largest 4 bins from the PCASP, so that the PCASP and SEM size distributions overlap. The SEM number distribution was higher than that of the PCASP in the four overlapping bins and a scaling factor was necessary to match the two. The whole SEM size distribution was then scaled down accordingly. The SEM technique is a 2-D procedure which measures geometrical diameter, and may overestimate particle diameters if the dust particles are nonspherical. Thus the scaling down of the SEM size distribution can partly be interpreted as accounting for this overestimation of diameter, as well as a conversion from geometrical to optical diameter. Errors in the PCASP size distribution due to the refractive index and particle shape might also intervene as estimated by *Osborne et al.* [2008], but are not able to account for the difference between the SEM and PCASP size distributions.

[27] Because of limitations with each technique we regard the various estimates of the coarse mode as a range of possibilities.

### 2.3. Dispersion Modeling Using NAME

[28] To identify potential dust sources, investigations were undertaken using the UK Met Office Numerical Atmospheric-dispersion Modeling Environment (NAME). This is a Lagrangian particle model [*Ryall and Maryon*, 1998] in which emissions from pollutant sources are represented by parcels released into a model atmosphere driven by the meteorological fields from the Met Office's numerical weather prediction model, the Unified Model [*Cullen*, 1993]. Each parcel carries the mass of one or more pollutant species and evolves by various physical and chemical processes during its lifespan. Although originally designed as an emergency response tool, NAME has subsequently been developed for a wide range of applications [e.g., *Middleton et al.*, 2008; *Gloster et al.*, 2007; *Webster et al.*, 2007; *Witham and Manning*, 2007].

[29] In this work two approaches have been taken. First, to identify potential source regions of the dust measured during DODO, NAME was initiated at a location where the aircraft had measured dust, and the air mass was run backward in time over 5 days in order to identify locations where the air mass had been in the lower boundary layer, within 200 m of the surface. While this technique highlights regions from which the air originated, it does not indicate

where dust was actually uplifted. In recent years a dust scheme has been developed [*Athanassiadou et al.*, 2006] in which dust is dynamically lifted, transported and deposited on the basis of the surface properties and meteorology. Therefore second, the relative contribution to the dust observed by the aircraft originating from different parts of the model domain have been identified by altering the extent of the modeled domain.

### 3. Identification of Aerosol Types

[30] The dominant aerosol types encountered during DODO were mineral dust (both campaigns) and biomass burning aerosols (DODO1 only). In order to isolate runs where the accumulation mode was dominated by dust only, we first removed runs where scattering from the nephelometer at 450 nm was greater than 550 nm and 700 nm, indicating the presence of biomass burning aerosol. For the remaining runs, we then looked at data from the aerosol mass spectrometer (AMS) and at the analysis of filter samples using scanning electron microscopy (SEM) and transmission electron microscopy (TEM). Analysis of air mass origin (see section 5) was not part of the selection criteria for dust cases, but the results support the hypothesis that the selected cases were dust aerosol, having sources in the Sahara and Sahel. However, we note that air mass origins do indicate that dust sampled during flights B173 and B174 had air mass origins around Spain and Portugal as well as in the northwest Sahara.

[31] Analysis of filter samples does not suggest any mixing of aerosol types or the presence of other components. Submicron mass loadings of organics and sulfates for DODO1 were determined using AMS data [see *Capes et al.*, 2008]. The dust cases described in this study have less than 15% of the submicron mass constituted by sulphates and organics, and can therefore be considered as dominated by dust in the accumulation mode, with the exception of run 3.1 in flight B174 where higher mass loadings of sulphates were found. On this basis, the aerosol samples presented are referred to as dust, on the assumption that mineral dust is almost certainly the dominant aerosol type and that mixing with other components is thought to be unlikely for the runs that have been selected.

### 4. Characteristics of Dust in DODO1 and DODO2

#### 4.1. Vertical Profiles

[32] Figure 5 shows the variety of vertical profiles of dust (and biomass burning aerosol) found during the DODO campaigns. In each case, the scattering coefficient at 550 nm, Angstrom exponent (calculated using the 550 and 700  $\mu\text{m}$  channels of the nephelometer), and ozone mixing ratio are shown. Small or even negative Angstrom exponent values imply larger particles (more likely to be dust), while larger positive values suggest small particles (more likely to be biomass burning or anthropogenic aerosol).

[33] Over land, close to the source, vertical profiles are quite similar for both the dry and wet season (Figures 5a and 5c), both showing a dust layer close to the surface. Figure 5a in the dry season (flight B175) shows a thick dust

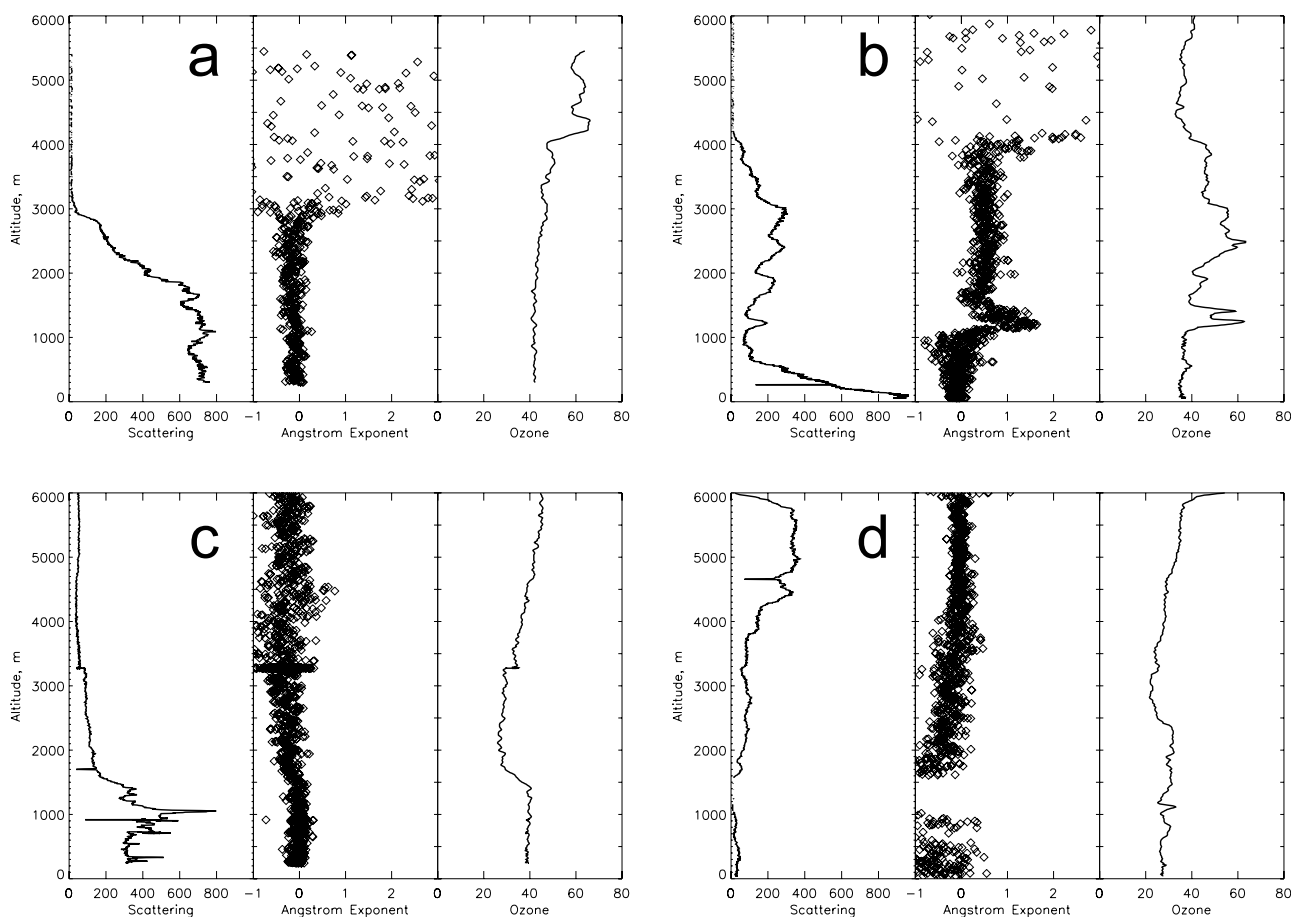


**Figure 5.** Vertical profiles of corrected 550 nm scattering ( $\text{Mm}^{-1}$ ), ozone mixing ratio (ppbv) and 550–700 nm Angstrom exponent for (a) B175 profile 7 (Mauritania, dry season), (b) B174 profile 6 (over ocean, dry season), (c) B238 profile 3 (Mauritania, wet season), and (d) B237 profile 2 (over ocean, wet season).

layer from the surface extending to 3000 m with the largest scattering toward ground level. The wet season (Figure 5c, flight B238) shows a similar layer also extending to around 3000 m, but with peak scattering at around 1000 m. Above 3000 m low scattering values ( $<100 \text{ Mm}^{-1}$ ) extend up to 6000 m, whereas in the dry season no aerosol was seen above 3000 m. Temperature and dew point temperature values (not shown) indicate that the boundary layer heights for these two profiles correspond to the altitude at which the scattering drops sharply, at around 3000 m for Figure 5a and around 6000 m for Figure 5c, although there is a minor inversion at around 1500 m, just above the scattering peak at 1000 m. Thus it appears that the differences in the vertical profiles of dust are due to seasonal variations in the height of the boundary layer, although the location of the profiles relative to the sources may also be a contributing factor.

[34] Figures 5b and 5d are profiles over the ocean from dry season (flight B174) and wet season (flight B237) respectively. During the dry season (Figure 5b) the scattering shows multiple layers of aerosol with one below 1000 m, and a second thicker layer, itself with considerable vertical structure, between 1500 m and 4000 m. The Angstrom exponent suggests different aerosol characteristics between these two layers with larger particles in the lower-altitude

layer. Ozone concentration is also positively correlated with the scattering in the upper layer, but not in the lower layer. This type of profile was common particularly during the more southerly flights in DODO1 and consists of a low-altitude layer of dust (present to varying degrees) and a higher-altitude layer of biomass burning aerosol (most likely mixed with some dust [e.g., Johnson *et al.*, 2008]). In contrast, during the wet season over the ocean (Figure 5d), there is no biomass aerosol present and instead there is a layer of weaker scattering from particles with a low Angstrom exponent between 4000 and 6000 m. The ozone shows an increase, as would be expected at altitude, but no positive correlation with the scattering as was observed in the winter season. The 4000 to 6000 m layer is presumably the Saharan Air Layer (SAL), containing mineral dust, which is uplifted by dry or moist convective activity over source regions to higher potential temperature surfaces, and then advected out over colder layers above the ocean. There is some evidence that the angstrom exponent decreases toward the ocean surface, suggesting the deposition of larger particles. The seasonal variation in aerosol profiles over the ocean will have important effects in terms of the longwave radiative effect, which depends on the altitude of the dust layer [e.g., Highwood *et al.*, 2003], and also in

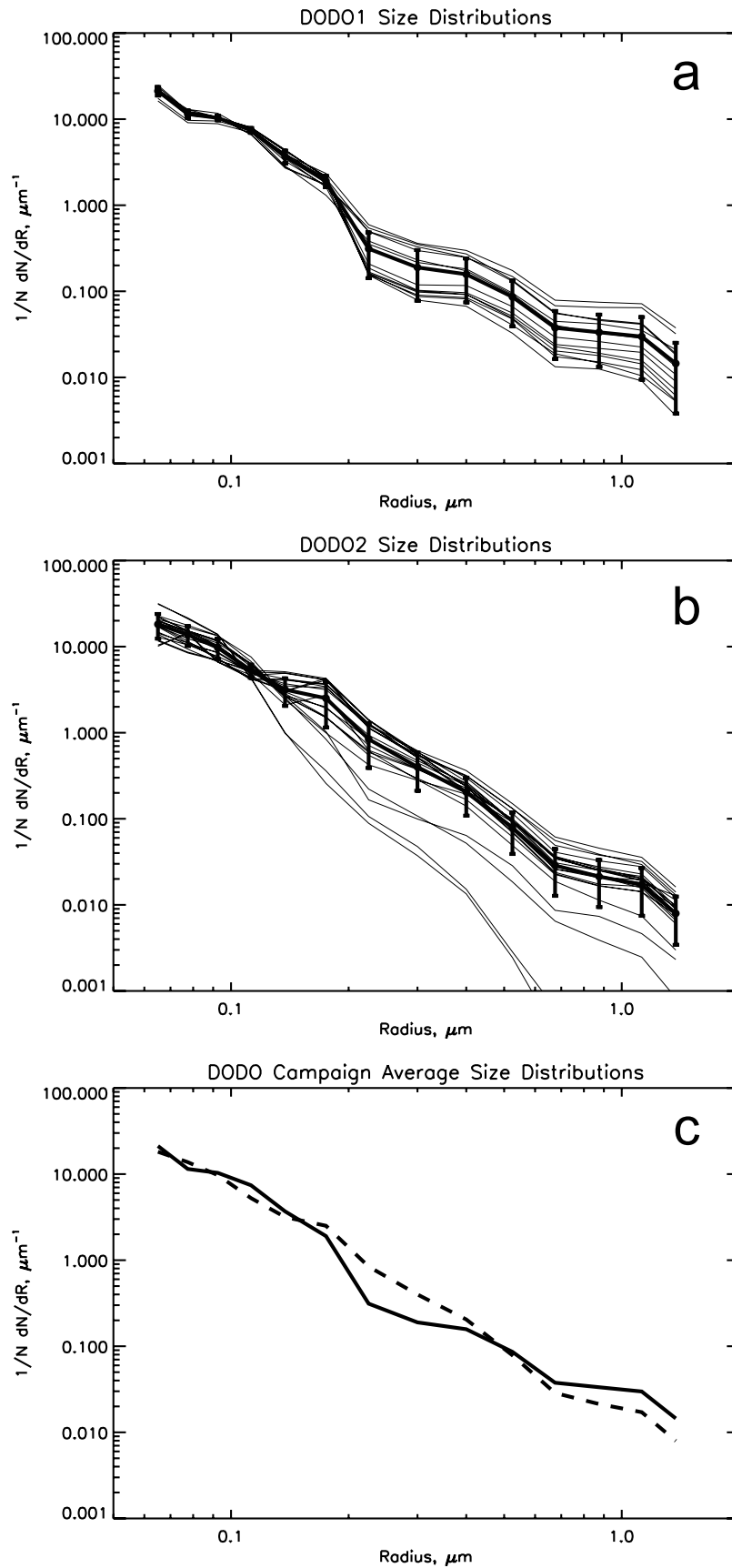


**Figure 6.** Size distributions measured by the PCASP on all runs dominated by dust, along with the average (heavy line) and errors (one standard deviation over each campaign) for (a) DODO1 and (b) DODO2. (c) Average size distributions for DODO1 (solid line) and DODO2 (dashed line).

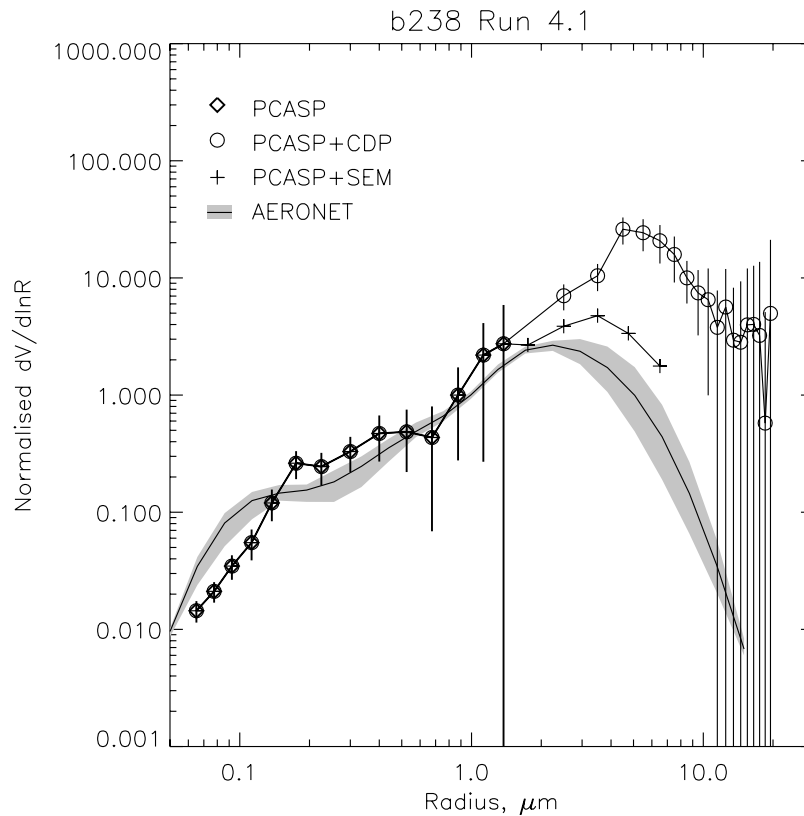


**Figure 7.** Volume size distributions for B238 run 4.1 at 1 km altitude on 23 August 2006 over Mauritania. The coarse mode was measured by a Cloud Droplet Probe (CDP) and by particle counting software used on Scanning Electron Microscope (SEM) imagery from filter samples. Size distributions from AERONET retrievals (Level 1.5, Version 2) are also shown. In order to compare distributions more meaningfully, in particular with AERONET, each distribution has been normalized by the value at 1  $\mu\text{m}$  radius (see text for details of processing).

terms of dust deposition to the ocean, a process which might be expected to take longer from a higher-altitude dust layer.

[35] Broadly the dust profiles are illustrative of what is known about the large-scale dynamics of this region of the atmosphere, clearly showing the elevated SAL in the wet season and low-level dust transport in the dry season [e.g., Chiapello *et al.*, 1995], although considerable variability within this idealized picture is evident, such as a deeper dust layer observed over land during the dry season (Figure 5b). A ubiquitous biomass burning haze was detected by the instrumentation and clearly visible by eye during almost all the flights throughout the dry season. The difference between vertical profiles of aerosol over land and ocean is apparent. Since determining vertical profiles of aerosol loading via remote sensing is challenging without recent developments in lidar technology, these profiles will provide a valuable opportunity for comparison with dust model results subsequently within the DODO project and beyond.

#### 4.2. Size Distribution

[36] Accumulation mode size distributions measured by the PCASP instrument for various straight and level runs in both DODO1 and DODO2 are shown in Figures 6a and 6b, with heavy lines showing campaign average size distributions. The average size distributions for DODO1 and DODO2 show small differences in the accumulation mode

between 0.2 and 0.6  $\mu\text{m}$  and 0.7–1.5  $\mu\text{m}$  radius (Figure 6c) between the two campaigns. Greater variability is seen in the DODO2 size distributions which can be at least partly associated with greater changes in size distribution over height of the dust layer.

[37] A significant coarse mode of dust is also present in some cases. Figure 7 shows the coarse mode size distributions, in terms of volume density, from run 4.1 at 1 km altitude during flight B238 (DODO2). This run is selected as an example when dust concentrations were high and data from both coarse mode instruments available. It should be noted that we are comparing optically equivalent sizes for the PCASP and CDP with geometric sizing from the SEM. Since most of the optical instruments are calibrated using latex spheres, if the aerosol being measured is substantially absorbing, then a correction will need to be made. DODO dust has been shown to be mainly scattering (see section 4.3) so we are assuming that the correction needed would be small, and within the considerable errors already described.

[38] The size distributions retrieved by inverting the scattered sky radiances measured by the Dakar AERONET site for the corresponding day are also shown, though it should be noted that these are column integrated measurements at a location around 580 km from the aircraft sampling region, and so could at best only be expected to

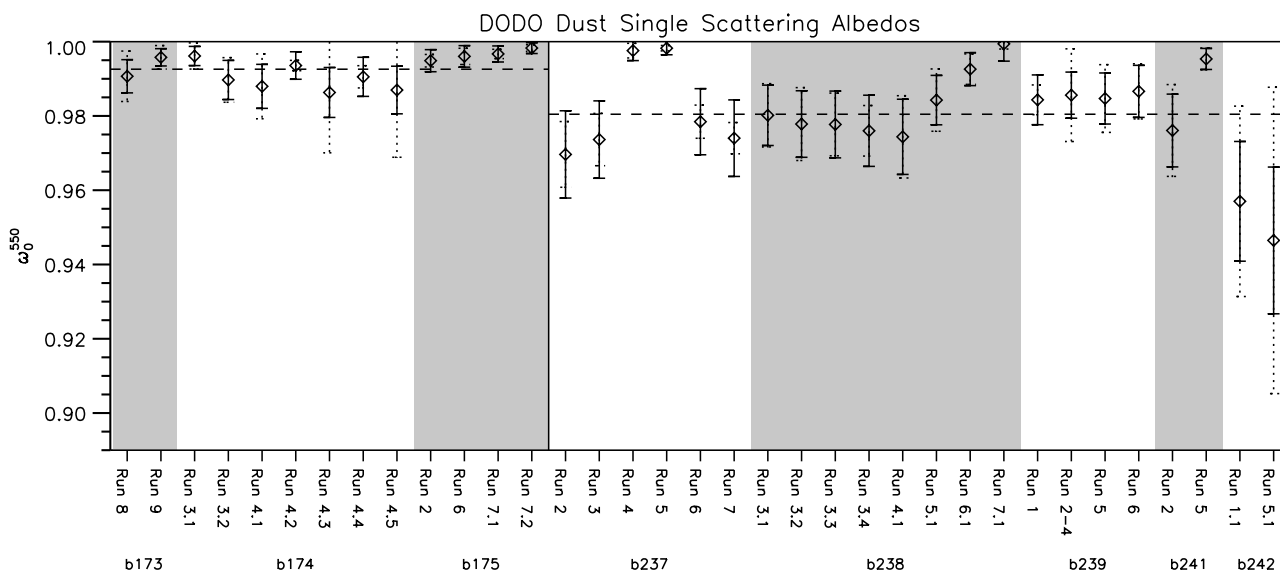


**Figure 8.** Accumulation mode single scattering albedos at 550 nm for each run in dust throughout the DODO campaigns, with errors estimated from variability across each run (dotted error bars) and from instrumental errors (solid error bars). Shaded/clear areas mark successive flights. Dashed horizontal lines show the campaign mean values of single scattering albedo as shown in Table 6. Single scattering albedos were calculated using absorption from the PSAP and scattering from the nephelometer, neither including contributions from the coarse mode.

be broadly similar to the aircraft measurements. In order to allow comparison between the in situ measurements and AERONET, each size distribution in Figure 7 is normalized by the value at  $1 \mu\text{m}$ . This avoids normalizing to the smallest bin of the PCASP which is known to be the least reliable of the PCASP size bins, or normalizing to the peak of the volume distribution which places too much faith in the coarse mode measurements given the large range shown.

[39] Although there are limitations associated with each measurement technique, it is important to note the large range of coarse mode volume distributions shown in Figure 7. The effects of this uncertainty arising from the different measurements of the coarse modes on optical properties are considered in section 4.4. The CDP and SEM size distributions show a different coarse mode both in terms of mode radius and magnitude, centered around  $4.5 \mu\text{m}$  and  $3.5 \mu\text{m}$  radius respectively. Considering the distance to the Dakar AERONET site, a distance greater than the assumed length scale of the dust outbreak indicated from satellite imagery (not shown), it is unsurprising that AERONET retrieves less coarse mode than the SEM and CDP. The accumulation modes show comparatively better agreement: at radii greater than  $0.2 \mu\text{m}$  agreement is achieved between AERONET and the PCASP size distributions within the bounds of the errors and variability shown. Below  $0.2 \mu\text{m}$  more particles are measured by AERONET than the aircraft.

### 4.3. Optical Properties

[40] Figure 8 shows the single scattering albedo values of dust-dominated cases from both campaigns, associated errors and campaign average single scattering albedos (see also Table 5). Results shown are averages measured during different aircraft runs which have been determined to be

dominated by dust (see section 3). As the PSAP and the nephelometer most likely measure absorption and scattering from the accumulation mode only, these results only show optical properties for the accumulation mode. Measured dust single scattering albedos were consistently high (always greater than 0.98) during DODO1, but showed greater variation during DODO2 ranging from 0.95 to 0.99. The variation observed during DODO2 could be attributed to both the variation in size distribution with altitude and to different dust sources and chemical composition. Although mixing or coating of dust with/by other aerosols or chemicals is a possibility, this was not evident from filter sample analysis.

[41] The campaign average mineral dust single scattering albedos for DODO1 and DODO2 accumulation mode were  $0.99 \pm 0.004$  and  $0.98 \pm 0.012$  respectively, with errors representing one standard deviation of the variability around the mean (see Table 5), (as opposed to the range of observed values shown in Figure 8). Hence DODO1 dust is slightly

**Table 5.** Lognormal Parameters for DODO Average Size Distributions (Accumulation Mode Only)

Mode	$r_g$ ( $\mu\text{m}$ )	$\sigma$	w
<i>DODO1</i>			
1	0.083	1.36	0.815
2	0.160	1.16	0.095
3	0.310	1.50	0.067
4	1.000	1.31	0.023
<i>DODO2</i>			
1	0.061	1.47	0.797
2	0.165	1.18	0.104
3	0.230	1.54	0.089
4	0.960	1.32	0.010

**Table 6.** Campaign Average Optical Properties From DODO, DABEX, and SHADE Campaigns<sup>a</sup>

	DODO1, Feb 2006		DODO2, Aug 2006		DABEX, Jan 2006	SHADE, Sep 2000
	Observations: AM	Mie: AM	Observations: AM	Mie: AM	[ <i>Osborne et al.</i> , 2008]: AM (AM + CM)	[ <i>Haywood et al.</i> , 2003]: AM (AM + CM)
$\omega_0^{550}$	$0.99 \pm 0.004$	0.99	$0.98 \pm 0.013$	0.98	0.99 (0.98)	0.97 (0.95)
Refractive index (550 nm)		$1.53 - 0.0005i$		$1.53 - 0.0014i$	$1.53 - 0.0004i$	$1.53 - 0.0015i$
$g^{550}$		0.68		0.68	0.71 (0.75)	0.72 (0.74)
$k_{\text{ext}}^{550}$ ( $\text{m}^2 \text{g}^{-1}$ )		0.85		1.14	0.76 (0.33)	0.70 (0.42)

<sup>a</sup>DODO observations are taken from the nephelometer and PSAP data, while the Mie results are from calculations using the observed size distributions for fine and accumulation mode particles only, assuming spherical dust and a refractive index to match the observed single scattering albedo. Errors on observed  $\omega_0^{550}$  indicate one standard deviation around the mean of values shown in Figure 8. CM indicates coarse mode, and AM indicates accumulation mode.

more scattering than DODO2 dust, though the errors do overlap. In comparison to other recent aircraft campaigns measuring North African dust, DABEX (January 2006, Niamey) measured consistently high  $\omega_0^{550}$  values with an average of 0.99 [*Osborne et al.*, 2008], and SHADE (September 2000 around the Capo Verde Islands) measured an average  $\omega_0^{550}$  of 0.97 with a range of 0.95–0.99 [*Haywood et al.*, 2003] (both campaigns accounting only for accumulation mode). These results, where dust has been determined to be the dominant aerosol type, suggest that the dry season dust has a higher  $\omega_0^{550}$  value than the wet season dust, for which  $\omega_0^{550}$  values seem to be more variable.

[42] The DODO measurements of  $\omega_0^{550}$  are at the upper end of previous estimates of  $\omega_0$ . Values of  $\omega_0^{670}$  for global dust range from 0.90 to 0.99, with an IPCC central global estimate of 0.96 [*Forster et al.*, 2007], with long-term AERONET estimates of  $\omega_0^{670}$  at 0.95 for Saharan dust [*Dubovik et al.*, 2002]. Note that the DODO calculations of single scattering albedo do not include the coarse mode contribution, the effect of which most likely decreases  $\omega_0$  by variable amounts (see section 4.4), depending on assumptions made about the composition of the coarse mode compared to the accumulation mode. Higher values of  $\omega_0^{550}$  impact the direct radiative effect in the shortwave by increasing the magnitude of the negative radiative effect at the TOA [*Forster et al.*, 2007].

[43] Table 6 shows the average optical properties (with associated errors) for both DODO1 and DODO2 calculated from Mie scattering code, as well as comparison to previous measurement campaigns. The measured size distributions (Figure 6) were fitted with four lognormal curves to produce a best fit curve (see Table 5). These were input into a Mie scattering code together with an inferred refractive index (constant with wavelength in the visible). The optical properties were retrieved, and the refractive index was chosen so that the single scattering albedo from Mie code matched that from observations. A density of  $2.65 \text{ g cm}^{-3}$  was assumed [*Teegen and Fung*, 1995] in order to calculate the mass specific extinction.

[44] The inferred refractive indices (Table 6) show that the DODO2 dust was more absorbing (higher imaginary part) than DODO1 dust. This suggests that the different campaign average single scattering albedos are explained by the dust composition (see section 5), since the size distributions are similar in the accumulation mode (see Figure 6c). Interestingly the refractive indices show similarities to the SHADE and DABEX campaigns both in terms of location

and season: both DODO1 and DABEX have low imaginary refractive indices showing very little absorption. In contrast, the wet season campaigns based around the West African coast produced higher imaginary refractive indices showing more absorption. These differences may be due to different dust sources having different mineralogy (in particular iron oxide amounts giving more absorption in the UV and midvisible parts of the spectrum in DODO2). Broadly the refractive indices from DODO fit in with the emerging picture from recent studies that North African dust has very low absorption [e.g., *Kaufman et al.*, 2001; *Dubovik et al.*, 2002; *Haywood et al.*, 2003; *Osborne et al.*, 2008].

[45] The asymmetry parameter calculated from Mie code for both DODO campaigns is 0.68, indicating that most radiation is scattered in a forward direction, and appears to differ little between campaigns. The mass specific extinction for the accumulation mode is significantly higher during DODO2 ( $1.14 \text{ m}^2 \text{ g}^{-1}$ ) showing that DODO2 accumulation mode dust is more efficient at extinguishing radiation per unit mass of aerosol. Mass specific extinction for DODO1 ( $0.85 \text{ m}^2 \text{ g}^{-1}$ ) is similar to that measured during SHADE and DABEX ( $0.76 \text{ m}^2 \text{ g}^{-1}$  and  $0.70 \text{ m}^2 \text{ g}^{-1}$ ). The higher value seen in DODO2 is possibly due to a greater proportion of mass between radii of 0.2–0.4  $\mu\text{m}$  where the dust is optically more efficient at extinguishing radiation.

#### 4.4. On the Role of the Coarse Mode for Calculation of Optical Properties

[46] Previous studies have shown that inclusion of the coarse mode when calculating optical properties of dust has a small effect, except in the calculation of mass specific extinction which drops significantly because of the large increase in mass when the coarse mode is included [*Haywood et al.*, 2003]. A sensitivity test was carried out to analyze the importance of the large coarse mode observed in flight B238 run 4.1 in calculating the optical properties, using the different measurements of coarse mode as shown in Figure 7.

[47] As described in section 4.3, Mie code was used to calculate the optical properties using the measured size distributions shown in Figure 7. Five lognormal modes were fitted to the measured size distributions using the coarse mode from each instrument as a sensitivity test in varying the amount of coarse mode present. The first four modes were fitted to the PCASP size distribution (repre-

**Table 7.** Optical Properties for B237 Run 4.1 at 1 km Altitude During DODO2, Showing the Effect of Including the Coarse Mode in the Calculation of Optical Properties<sup>a</sup>

Instrument Measuring Coarse Mode	$\omega_0^{550}$	$g^{550}$	$K_{\text{ext}}^{550}$ ( $\text{m}^2 \text{g}^{-1}$ )
No coarse mode (PCASP only)	0.98	0.69	1.22
SEM	0.96	0.72	0.46
CDP	0.90	0.77	0.20

<sup>a</sup>PCASP only results exclude the effect of the coarse mode, and use four lognormals to fit to the size distribution. Size distributions using the SEM and CDP use the same four lognormal modes for the accumulation mode but include a fifth to fit the coarse mode which is derived from each measurement.

senting the accumulation mode) and remained identical in each case. The fifth mode was fitted to the coarse mode from each instrument and the parameters of this mode changed depending on which instrument was measuring the coarse mode. The refractive index was calculated specifically for the accumulation mode dust sampled in run 4.1 and was applied to the whole size distribution.

[48] Table 7 shows the results of the effects of the different coarse modes on the optical properties of the dust. As found previously, the addition of the coarse mode decreases  $\omega_0^{550}$ , increases  $g$  and decreases  $K_{\text{ext}}^{550}$  [Haywood *et al.*, 2003]. The DODO results show that the changes in the optical properties are more marked when a greater amount of coarse mode is present, as with the CDP. For example,  $\omega_0^{550}$  decreases from 0.98 to 0.90 with the addition of the CDP coarse mode, a substantial change. Less of a decrease in  $\omega_0^{550}$  is observed when less coarse mode is measured. The mass specific extinction changes similarly with the varying amounts of coarse mode. Thus the optical properties in this case are extremely sensitive to the amount and presence of the coarse mode. In this illustrative example it has been assumed that the refractive index of the dust (and therefore the composition) of coarse and accumulation modes are the same. If there were dramatically different sources or composition then the impact on the optical properties could be different to that described. SEM and TEM analysis on a small number of particles for this case showed some differences of composition between the accumulation and coarse modes. In particular the accumulation mode contained iron oxides which were not measured in the coarse mode. Iron oxides such as hematite and goethite are responsible for absorption of UV and visible light [Sokolik and Toon, 1999; Lafon *et al.*, 2006]. Future work will involve a more sophisticated representation of refractive index with particle size. Meanwhile these results show that accurate measurement of the coarse mode in mineral dust is extremely important and so in future aircraft studies effort must be made in operating fully calibrated aerosol probes that can measure particles sizes up to 10–20  $\mu\text{m}$  radius.

## 5. Dust Source Identification

[49] Elemental concentrations for the combined accumulation and coarse modes were measured by particle induced X-ray emission (PIXE) at the Laboratorio di Tecniche Nucleari per i Beni Culturali (LABEC) [Chiari *et al.*, 2005; Calzolari *et al.*, 2006]. Ratios of elemental concen-

trations usually associated with dust have been calculated for the same cases as those described in sections 3 and 4, and are shown in Table 8. Average elemental ratios for Si/Al are  $2.7 \pm 0.2$  for DODO1 and  $2.6 \pm 0.3$  for DODO2. These are all somewhat higher than previous SHADE results from Formenti *et al.* [2003], and from the range of results for different origins given by Chiapello [1996], but less than the value in crustal rock [Mason, 1966]. It is possible that transport as well as source regions affects this ratio, since some of DODO1 and DODO2 samples were much closer to the source of the dust than those in the previous studies. It is also possible that the source area of the dust has different characteristics.

[50] DODO1 shows substantially higher Ca/Al ratio ( $1.1 \pm 0.4$ ) compared to DODO2 ( $0.5 \pm 0.2$ ), indicating that the DODO1 samples had sources based more toward the northern Sahara than DODO2 [e.g., Formenti *et al.*, 2008; J. L. Rajot *et al.*, AMMA dust experiment: An overview of measurements during the dry season special observation period (SOP 0) at the Banizoumbou (Niger) supersite, submitted to *Journal of Geophysical Research*, 2008]. The K/Al ratio is  $0.3 \pm 0.1$  for DODO1 and  $0.2 \pm 0.1$  for DODO2: again DODO2 is similar to results for Saharan dust from Chiapello [1996]. Finally, Fe/Al ratios are  $0.7 \pm 0.1$  for both DODO1 and DODO2, slightly higher than was found during SHADE by Formenti *et al.* [2003] and by Chiapello [1996]. Formenti *et al.* [2008] have shown that the Fe/Al ratio is not that sensitive to the source region. Conversely, these authors indicate that the iron oxide to iron ratio is more sensitive to source region.

[51] The elemental analysis of filter samples and optical property results suggest some differences in source characteristics between DODO1 and DODO2, and between different dust samples collected from different (and sometimes the same) flights. NAME was run for several cases for both DODO campaigns in order to determine potential dust source regions. Figure 9 shows air mass origins from the NAME for dust sampled during different runs from two flights (B175 in DODO1 and B238 in DODO2) over Mauritania.

[52] For the flights and runs shown, the dust encountered during DODO1 straight and level runs originated (over a 5 day period) from more geographically limited regions than that encountered during DODO2. Figure 9a shows the air mass origin from B175 (run 7.2 at 170 m above ground level), and suggests potential dust sources originating from the boundary layer in Algeria and Mauritania. Dust found at similar altitudes and geographical locations during DODO2 flight B238 (run 3.3) suggested that the air mass originated from more coastal regions of western Sahara and Morocco (Figure 9b). There is a substantial difference in single scattering albedo between these runs, with that from DODO2 being lower. Although mixing with anthropogenic aerosol from Spain or Portugal could be a factor (though it was not

**Table 8.** Mean Elemental Ratios Measured by PIXE for Filter Samples From DODO<sup>a</sup>

	Si/Al	Ca/Al	K/Al	Fe/Al
DODO1 dust	2.7 (0.2)	1.1 (0.4)	0.3 (0.1)	0.7 (0.1)
DODO2 dust	2.6 (0.3)	0.5 (0.2)	0.2 (0.1)	0.7 (0.1)

<sup>a</sup>Values in parentheses represent one standard deviation.

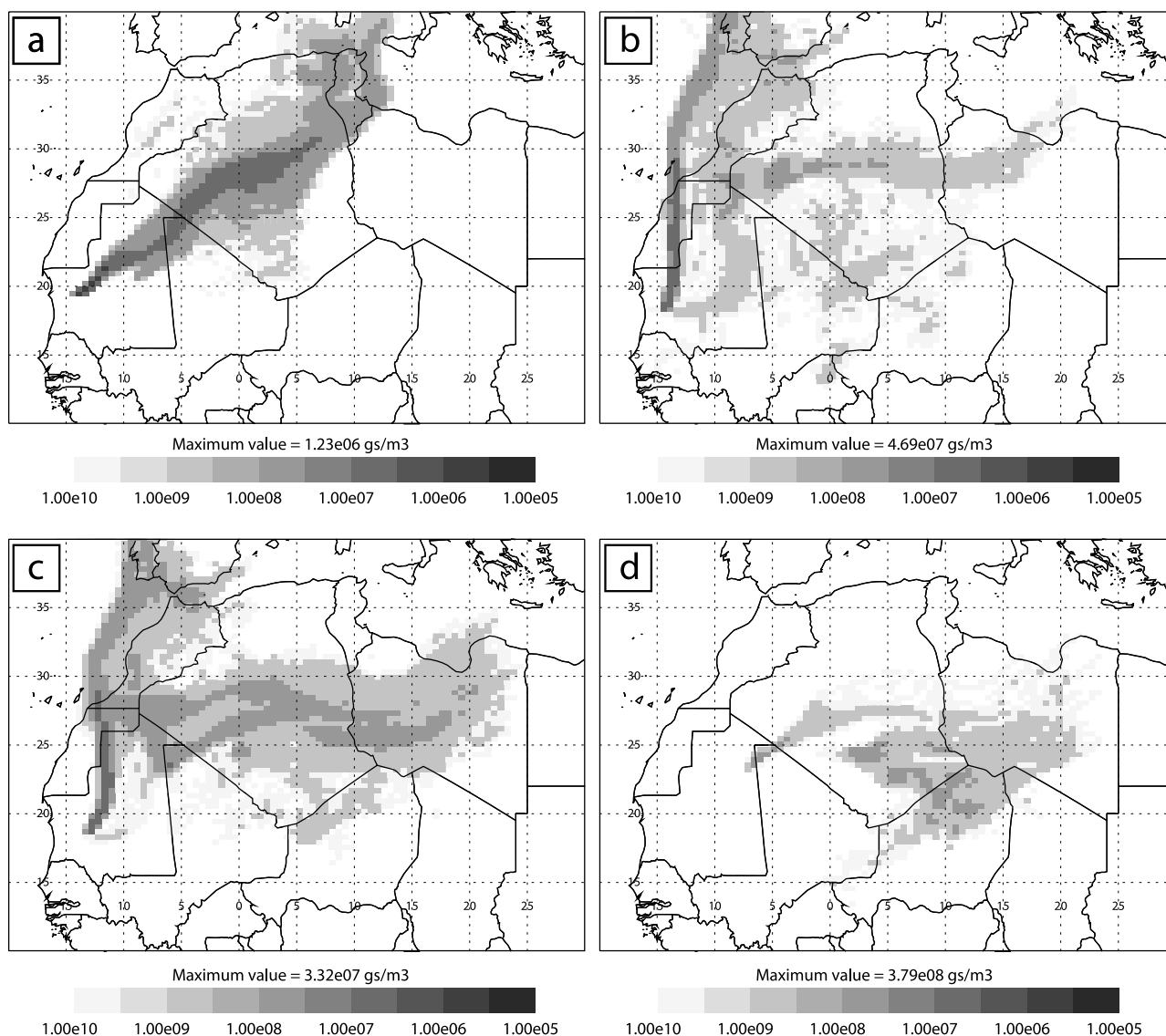


**Figure 9.** Five day particle release experiments from the UK Met Office NAME model, indicating the likely origin (within the lowest 200 m) of dust encountered during straight and level runs of the BAe146 aircraft. (a) DODO1 B175 run 7.2 at 175 m above ground level (agl), (b) DODO2 B238 run 3.3 at 175 m agl, (c) DODO2 B238 run 5.1 at 2 km agl, and (d) DODO2 B238 run 7.1 at 5 km agl.

evident on filter samples), the lower single scattering albedo is likely due to the mineralogy of the dust since *Formenti et al.* [2008] found high values of absorbing iron oxides for this run.

[53] Analysis of air mass origins for dust encountered during other straight and level runs in flight B238 over northern Mauritania suggests different source regions for each dust layer at different altitudes. At around 2 km (run 5.1) the dust appears to have originated from a mixture of locations including a well-defined area within Mauritania, coastal regions around Morocco, and central Algeria and western Libya (Figure 9c). Dust from within the highest altitude in the SAL at around 5.2 km (run 7.1) has 5 day origins further west around northern Niger, southern Algeria and southwest Libya (Figure 9d). Thus for the case of B238 dust encountered higher up in the atmosphere is likely to have originated from sources further east than sources at lower altitudes.

[54] NAME simulations for the other flights (not shown) show similar patterns in the air mass origins. DODO1 dust (dry season) was always transported by air masses originating from the north to northwest within a narrow plume (as shown in Figure 9a), whereas the DODO2 (wet season) potential dust sources were much more widespread over North Africa, as indicated by the variation in potential sources shown in Figures 9b–9d. This difference could be explained by the small number of dust events encountered during DODO1, with similar meteorology during each, rather than being a truly seasonal effect.

[55] Different dust sources are expected to have different mineralogy and therefore different optical properties [e.g., *Claquin et al.*, 1999; *Caquineau et al.*, 2002]. It is therefore interesting that both the single scattering albedos shown in Figure 8 and the potential dust sources for DODO2 dust cases show more variability than those for DODO1, and suggests that the dust mineralogy or source region is having

an important effect on the optical properties observed. Notably the air mass origins for dust sampled during flight B242 (not shown) appear to be from further south than those for other flights, with potential sources being centered around southern Algeria, eastern Mali and northwestern Niger. This coincides with single scattering albedos for this flight being much lower than those for other flights. It is possible that the mineralogy of dust sampled during this flight is rather different to others, possibly because of higher concentrations of absorbing iron oxides in sources located further south [Clauquin *et al.*, 1999; Alfaro *et al.*, 2004; Lafon *et al.*, 2006]. Further work will examine the mineralogy from flight B242 in more detail.

[56] Care must be taken in interpreting these results, since although the air masses may have passed through these potential source areas this does not necessarily mean that dust has been uplifted. In order to account for this for the case of flight B238, forward model runs were undertaken incorporating the dust uplift scheme. Results indicate that essentially all the dust observed at low altitude (run 3.3) originated from the region west of 0E. This region accounted for approximately 80% of the dust observed at mid levels (run 5.1) but only 10% of that observed at high levels (run 7.1), with the remainder having been transported from further east. Therefore the hypothesis that for the case of flight B238 the high-altitude dust had been transported over larger distances than the dust sampled at lower altitudes, and that the high-altitude dust had different dust sources to the dust at low altitudes, as indicated by the air mass origins from NAME, is supported by the dust model results.

## 6. Discussion and Future Plans

[57] Aircraft observations of North African dust during the DODO project reveal some interesting differences between wet and dry season dust during 2006. Differences in the measured accumulation mode  $\omega_0^{550}$  for dust between the dry and wet season campaigns suggest higher values of  $\omega_0^{550}$  are more prevalent during the dry season (0.99 (0.98–0.999), DODO1), while wet season  $\omega_0^{550}$  values are more variable (0.98 (0.94–0.999) DODO2) and slightly lower on average. This range of observed single scattering albedos will be important in terms of the radiative effect. Potential dust sources suggested by NAME are also more variable during DODO2, whereas during DODO1 they were more confined in area and located in the northwest Sahara. Of the elemental ratios examined those of Ca/Al were the most variable between the DODO campaigns, with higher values observed during DODO1, also suggesting dust sources further toward the northern Sahara. Changes in such ratios also have implications for minerals deposited to the ocean. The size distributions for the accumulation mode were less variable between campaigns and flights. Thus the available data suggests that the different optical properties of the accumulation mode between the two DODO campaigns are related to the chemical composition of the dust and the potential dust sources. This also is reflected in the different derived refractive index for the accumulation mode between campaigns; 1.53–0.0005i for DODO1 and 1.53–0.0014i for DODO2. Mineralogical information will be used to confirm the consistency of our inferred refractive indices

with the observed composition. We note that the correction of the BAe146 nephelometer based on the DC-8 nephelometer involves some uncertainty based on the uncertainty in the passing efficiency of the Rosemount inlets on the BAe146 relative to those of the DC-8, and that there is therefore a degree of uncertainty in the measured optical properties for the DODO2 accumulation mode results.

[58] Aerosol optical depth estimates from the aircraft extinction profiles in general underestimated those from AERONET (values shown in Table 4). Differences were within a factor of 1.5 for DODO1, and to within 1.35 during DODO2 once correction had been made to DODO2 values on the basis of a poorly behaving nephelometer and comparison with the NASA DC-8. These ratios to AERONET are consistent with previous work from SHADE [Haywood *et al.*, 2003] and are attributed to loss of coarse mode particles in the aircraft inlets. During DABEX, Osborne *et al.* [2008] found that once corrected for missing scattering based on measurements of the coarse mode the aircraft extinction tended to overestimate dust optical depth compared to AERONET data at Banizoumbou.

[59] The importance of the coarse mode in affecting radiative properties is apparent in DODO, as is the lack of adequately validated airborne measurements. While the single scattering albedo for the accumulation mode was measured directly, we must rely on size distribution measurements in order to calculate the single scattering albedo for the combined accumulation and coarse modes. We have presented size distributions from two different techniques for measuring the coarse mode, both of which have limitations. We illustrate that the uncertainty from different coarse mode size distributions results in a large variation in the single scattering albedo of dust (0.90 with the largest coarse mode to 0.98 with no coarse mode present), although here we make the simple assumption that the coarse mode composition is the same as that of the accumulation mode. This is an area where development is required in order to reduce the uncertainty in key properties such as the single scattering albedo and hence the radiative effect of dust. Large-scale dust events such as the March 2006 dust storm are likely to have a substantial coarse mode, which could lead to significantly different values of single scattering albedo and may explain differences previously reported [Slingo *et al.*, 2006; Haywood *et al.*, 2003].

[60] The vertical profiles measured during DODO are qualitatively consistent with what would be expected on the basis of the differing meteorology of the two seasons. (e.g., Chiapello *et al.* [1995] (winter transport at low altitudes) and Karyampudi *et al.* [1999] (wet season transport in SAL), and Zhu *et al.* [2007] (comparison of dust plumes in different seasons)). When present, dry season dust was always found at low altitudes, whereas wet season dust was found to be transported up to altitudes of 6 km. However, during one flight in the dry season dust was found in a layer extending up to around 3 km over the land (flight B175), implying that there may be substantial variability in the idealized picture. A ubiquitous layer of biomass burning aerosol was found aloft during the dry season to the south of Dakar.

[61] The optical properties of dust aerosol are crucial in determining the radiative effect of dust accurately [Haywood and Shine, 1995] and so variations in the single scattering

albedo such as those presented here are extremely important. Further work will assess the radiative effect of the dust sampled during both DODO campaigns, using both radiometer data from the aircraft and a radiative transfer code. Finally, the iron content will be assessed in more detail as this is relevant for converting the deposition of dust in general to the ocean to a contribution of iron.

[62] There are obvious limitations to using only 1 year for a comparison. However, we believe the results presented here are of wider applicability since the flow during DODO2 was climatological and during DODO1 the analysis of dust samples was completed on days when the flow was climatological. Additionally, the campaign suffered from some major uncertainties in the behavior of key instrumentation. However, having made best attempts with independent data to quantify and assess the reasons for necessary corrections, these observations add to the available data on North African dust. The case studies are being used to constrain numerical models of dust uplift and transport which will ultimately be used to assess the deposition of dust to the Atlantic Ocean. Dust is a crucial part of the climate system, acting as a forcing and involved in feedbacks between anthropogenic and natural climate change mechanisms. However, the processes involved in dust uplift are many and occur at small spatial scales and are often episodic in nature. The use of integrated airborne, ground and remote sensing measurements to constrain models is a vital step forward in our ability to model dust distributions, and for this there must be a continuation of long-term monitoring of dust properties such as by AERONET and AMMA dust stations, supplemented by in situ aircraft campaigns covering as many seasons and locations as is feasible.

[63] **Acknowledgments.** DODO is funded by NERC via the SOLAS directed program (grant NE/C517276/1). The aircraft campaigns would not have been possible without the professional and enthusiastic staff of FAAM, DirectFlight, and Avalon Engineering. We also acknowledge the support and staff of the Met Office who were involved in these campaigns and in discussion of the analysis. FAAM is jointly funded by the Natural Environment Research Council and the Met Office. The financial support of the French API-AMMA national program to the chemical and microscopy analysis of the bulk filter samples is also acknowledged. The CDP is not a core FAAM instrument and we would like to acknowledge the provision of the CDP data by Martin Gallagher through the support of the IAGOS project. We thank the AERONET PI Didier Tanré for his effort in establishing and maintaining the Dakar AERONET site.

## References

- Abel, S. (2007), CDP airflow modelling and droplet shadowing on the FAAM 146, paper presented at FAAM Cloud Instrument User Group Meeting, Univ. of Manchester, Manchester, U. K., 10 Oct. (Available at [http://web.mac.com/mccssmwg1/CIUG/Presentations\\_1.html](http://web.mac.com/mccssmwg1/CIUG/Presentations_1.html))
- Alfaro, S. C., S. Lafon, J. L. Rajot, P. Formenti, A. Gaudichet, and M. Maille (2004), Iron oxides and light absorption by pure desert dust: An experimental study, *J. Geophys. Res.*, *109*, D08208, doi:10.1029/2003JD004374.
- Anderson, T. L., and J. A. Ogren (1998), Determining aerosol radiative properties using the TSI 3563 integrating nephelometer, *Aerosol Sci. Technol.*, *29*(1), 57–69, doi:10.1080/02786829808965551.
- Andreae, M. O., et al. (2000), Soluble ion chemistry of the atmospheric aerosol and SO<sub>2</sub> concentrations over the eastern North Atlantic during ACE-2, *Tellus, Ser. B*, *52*(4), 1066–1087, doi:10.1034/j.1600-0889.2000.00105.x.
- Athanassiadou, M., H. Floccas, M. A. J. Harrison, M. C. Hort, C. S. Witham, and S. Watkin (2006), The dust event of 17 April 2005 over Athens, Greece, *Weather*, *61*(5), 125–131.
- Bond, T. C., T. L. Anderson, and D. Campbell (1999), Calibration and intercomparison of filter-based measurements of visible light absorption by aerosols, *Aerosol Sci. Technol.*, *30*, 582–600, doi:10.1080/027868299304435.
- Calzolari, G., M. Chiari, I. Garcia Orellana, F. Lucarelli, A. Migliori, S. Nava, and F. Taccetti (2006), The new external beam facility for environmental studies at the Tandem accelerator of LABEC, *Nucl. Instrum. Methods in Phys. Res., Sect. B*, *249*, 928–931.
- Capes, G., B. T. Johnson, G. McFiggans, P. I. Williams, J. M. Haywood, and H. Coe (2008), Aging of biomass burning aerosols over West Africa: Aircraft measurements of chemical composition, microphysical properties and emission ratios, *J. Geophys. Res.*, doi:10.1029/2008JD009845, in press.
- Caquiereau, S., A. Gaudichet, L. Gomes, and M. Legrand (2002), Mineralogy of Saharan dust transported over northwestern tropical Atlantic Ocean in relation to source regions, *J. Geophys. Res.*, *107*(D15), 4251, doi:10.1029/2000JD000247.
- Carrico, C. M., P. Kus, P. K. Quinn, and T. S. Bates (2003), Mixtures of pollution, dust, sea salt, and volcanic aerosol during ACE-Asia: Radiative properties as a function of relative humidity, *J. Geophys. Res.*, *108*(D23), 8650, doi:10.1029/2003JD003405.
- Chiapello, I. (1996), Les aérosols atmosphériques au-dessus de l'Atlantique nord tropical: Approche physico-chimique et météorologique. Evaluation de la contribution de différentes espèces à l'épaisseur optique en aérosol, Ph.D. thesis, Univ. Paris VII, Paris.
- Chiapello, I., G. Bergametti, L. Gomes, B. Chatenet, F. Dulac, J. Pimenta, and E. Santos Soares (1995), An additional low layer transport of Sahelian and Saharan dust over the northeastern tropical Atlantic, *Geophys. Res. Lett.*, *22*(23), 3191–3194, doi:10.1029/95GL03313.
- Chiapello, I., G. Bergametti, B. Chatenet, P. Bousquet, F. Dulac, and E. Santos Soares (1997), Origins of African dust transported over the northeastern tropical Atlantic, *J. Geophys. Res.*, *102*(D12), 13,701–13,709, doi:10.1029/97JD00259.
- Chiari, M., F. Lucarelli, F. Mazzei, S. Nava, L. Paperetti, P. Prati, G. Valli, and R. Vecchi (2005), Characterization of airborne particulate matter in an industrial district near Florence by PIXE and PESA, *X Ray Spectrom.*, *34*(4), 323–329, doi:10.1002/xrs.825.
- Chou, C., P. Formenti, M. Maille, P. Ausset, G. Helas, M. Harrison, and S. Osborne (2008), Size distribution, shape and composition of mineral dust aerosols collected during the AMMA SOP0/DABEX field campaign in Niger, January 2006, *J. Geophys. Res.*, doi:10.1029/2008JD009897, in press.
- Claquin, T., M. Schulz, and Y. J. Balkanski (1999), Modeling the mineralogy of atmospheric dust sources, *J. Geophys. Res.*, *104*(D18), 22,243–22,256, doi:10.1029/1999JD900416.
- Cullen, M. J. P. (1993), The unified forecast/climate model, *Meteorol. Mag.*, *122*, 81–93.
- DeMott, P. J., K. Sassen, M. R. Poellot, D. Baumgardner, D. C. Rogers, S. D. Brooks, A. J. Prenni, and S. M. Kreidenweis (2003), African dust aerosols as atmospheric ice nuclei, *Geophys. Res. Lett.*, *30*(14), 1732, doi:10.1029/2003GL017410.
- Dubovik, O., B. Holben, T. F. Eck, A. Smirnov, Y. Kaufman, M. D. King, and D. Tarré (2002), Variability of absorption and optical properties of key aerosol types observed in worldwide locations, *J. Atmos. Sci.*, *59*, 590–608.
- Engelstaedter, S., and R. Washington (2007), Atmospheric controls on the annual cycle of North African dust, *J. Geophys. Res.*, *112*, D03103, doi:10.1029/2006JD007195.
- Evan, A., J. A. Dunion, J. A. Foley, A. K. Heidinger, and C. S. Velden (2006), New evidence for a relationship between Atlantic tropical cyclone activity and African dust outbreaks, *Geophys. Res. Lett.*, *33*, L19813, doi:10.1029/2006GL026408.
- Field, P. R., O. Mohler, P. Connolly, M. Kramer, R. Cotton, A. J. Heymsfield, H. Saathoff, and M. Schnaiter (2006), Some ice nucleation characteristics of Asian and Saharan desert dust, *Atmos. Chem. Phys.*, *6*, 2991–3006.
- Formenti, P., M. O. Andreae, L. Lange, G. Roberts, J. Cafmeyer, I. Rajta, W. Maenhaut, B. N. Holben, P. Artaxo, and J. Lelieveld (2001), Saharan dust in Brazil and Suriname during the Large-Scale Biosphere-Atmosphere Experiment in Amazonia (LBA)–Cooperative LBA Regional Experiment (CLAIRE) in March 1998, *J. Geophys. Res.*, *106*(D14), 14,919–14,934, doi:10.1029/2000JD900827.
- Formenti, P., W. Elbert, W. Maenhaut, J. Haywood, and M. O. Andreae (2003), Chemical composition of mineral dust aerosol during the Saharan Dust Experiment (SHADE) airborne campaign in the Cape Verde region, September 2000, *J. Geophys. Res.*, *108*(D18), 8576, doi:10.1029/2002JD002648.
- Formenti, P., et al. (2008), Composition of mineral dust from western Africa: Results from the AMMA SOP0/DABEX and DODO field campaigns, *J. Geophys. Res.*, doi:10.1029/2008JD009903, in press.
- Forster, P., et al. (2007), Changes in atmospheric constituents and in radiative forcing, in *Climate Change 2007: The Physical Science Basis—Contribution of Working Group I to the Fourth Assessment Report of*

- the Intergovernmental Panel on Climate Change, edited by S. Solomon et al., pp. 130–234, Cambridge Univ. Press, New York.
- Gloster, J., P. S. Mellor, A. J. Manning, H. N. Webster, and M. C. Hort (2007), Assessing the risk of windborne spread of bluetongue in the 2006 outbreak of disease in northern Europe, *Vet. Rec.*, *160*, 54–56.
- Hastenrath, S. (1991), *Climate Dynamics of the Tropics*, Kluwer Acad., Dordrecht, Netherlands.
- Haywood, J., and K. Shine (1995), The effect of anthropogenic sulfate and soot aerosol on the clear sky planetary radiation budget, *Geophys. Res. Lett.*, *22*(5), 603–606, doi:10.1029/95GL00075.
- Haywood, J., P. Francis, S. Osborne, M. Glew, N. Loeb, E. Highwood, D. Tarré, G. Myhre, P. Formenti, and E. Hirst (2003), Radiative properties and direct radiative effect of Saharan dust measured by the C-130 aircraft during SHADE: 1. Solar spectrum, *J. Geophys. Res.*, *108*(D18), 8577, doi:10.1029/2002JD002687.
- Highwood, E. J., J. M. Haywood, M. D. Silverstone, S. M. Newman, and J. P. Taylor (2003), Radiative properties and direct effect of Saharan dust measured by the C-130 aircraft during Saharan Dust Experiment (SHADE): 2. Terrestrial spectrum, *J. Geophys. Res.*, *108*(D18), 8578, doi:10.1029/2002JD002552.
- Jickells, T. D., et al. (2005), Global iron connections between desert dust, ocean biogeochemistry, and climate, *Science*, *308*(5718), 67–71, doi:10.1126/science.1105959.
- Johnson, B. T., S. R. Osborne, and J. M. Haywood (2008), Aircraft measurements of biomass burning aerosols over West Africa during DABEX, *J. Geophys. Res.*, doi:10.1029/2007JD009741, in press.
- Jones, C., N. Mahowald, and C. Luo (2004), Observational evidence of African desert dust intensification of easterly waves, *Geophys. Res. Lett.*, *31*, L17208, doi:10.1029/2004GL020107.
- Karyampudi, V. M., et al. (1999), Validation of the Saharan Dust Plume conceptual model using Lidar, Meteosat and ECMWF Data, *Bull. Am. Meteorol. Soc.*, *80*, 1045–1074, doi:10.1175/1520-0477(1999)080<1045:VOTSDP>2.0.CO;2.
- Kaufman, Y. J., D. Tarré, O. Dubovik, A. Karneili, and L. A. Remer (2001), Absorption of sunlight by dust as inferred from satellite and ground-based remote sensing, *Geophys. Res. Lett.*, *28*(8), 1479–1482.
- Lafon, S., I. N. Sokolik, J. L. Rajot, S. Caquineau, and A. Gaudichet (2006), Characterization of iron oxides in mineral dust aerosols: Implications for light absorption, *J. Geophys. Res.*, *111*, D21207, doi:10.1029/2005JD007016.
- Li-Jones, X., H. B. Maring, and J. M. Prospero (1998), Effects of relative humidity on light scattering by mineral dust aerosol as measured in the marine boundary layer over the tropical Atlantic Ocean, *J. Geophys. Res.*, *103*(D23), 31,113–31,121, doi:10.1029/98JD01800.
- Magi, B. I., and P. V. Hobbs (2003), Effects of humidity on aerosols in southern Africa during the biomass burning season, *J. Geophys. Res.*, *108*(D13), 8495, doi:10.1029/2002JD002144.
- Mason, B. (1966), *Principles of Geochemistry*, 3rd ed., John Wiley, Hoboken, N. J.
- McNaughton, C. S., et al. (2007), Results from the DC-8 inlet Characterisation Experiment (DICE): Airborne versus surface sampling of mineral dust and sea salt aerosols, *Aerosol Sci. Technol.*, *41*(2), 136–159, doi:10.1080/02786820601118406.
- Middleton, D. R., A. R. Jones, A. L. Redington, D. J. Thomson, R. S. Sokhi, L. Luhana, and B. E. A. Fisher (2008), Lagrangian modelling of plume chemistry for secondary pollutants in large industrial plumes, *Atmos. Environ.*, *42*, 415–427, doi:10.1016/j.atmosenv.2007.09.056.
- Osborne, S., B. Johnson, J. Haywood, C. McConnell, A. J. Baran, and M. A. J. Harrison (2008), Physical and optical properties of mineral dust aerosol during the Dust and Biomass Experiment (DABEX), *J. Geophys. Res.*, doi:10.1029/2007JD009551, in press.
- Prospero, J. M. (1999), Long-term measurements of the transport of African mineral dust to the southeastern United States: Implications for regional air quality, *J. Geophys. Res.*, *104*(D13), 15,917–15,927.
- Redelsperger, J.-L., C. D. Thorncroft, A. Diedhiou, T. Lebel, D. J. Parker, and J. Polcher (2006), African monsoon multidisciplinary analysis: An international research project and field campaign, *Bull. Am. Meteorol. Soc.*, *87*(12), 1739–1746, doi:10.1175/BAMS-87-12-1739.
- Reid, J. S., et al. (2003), Analysis of measurements of Saharan dust by airborne and ground-based remote sensing methods during the Puerto Rico Dust Experiment (PRIDE), *J. Geophys. Res.*, *108*(D19), 8586, doi:10.1029/2002JD002493.
- Richardson, M. S., et al. (2007), Measurements of heterogeneous ice nuclei in the western United States in springtime and their relation to aerosol characteristics, *J. Geophys. Res.*, *112*, D02209, doi:10.1029/2006JD007500.
- Ryall, D. B., and R. H. Maryon (1998), Validation of the UK Met Office's NAME model against the ETEX dataset, *Atmos. Environ.*, *32*, 4265–4276, doi:10.1016/S1352-2310(98)00177-0.
- Salisbury, G., J. Williams, V. Gros, S. Bartenbach, X. Xu, H. Fischer, R. Kormann, M. de Reus, and M. Zöllner (2006), Assessing the effect of a Saharan dust storm on oxygenated organic compounds at Izaña, Tenerife (July–August 2002), *J. Geophys. Res.*, *111*, D22303, doi:10.1029/2005JD006840.
- Schepanski, K., I. Tegen, B. Laurent, B. Heinold, and A. Macke (2007), A new Saharan dust source activation frequency map derived from MSG-SEVIRI IR-channels, *Geophys. Res. Lett.*, *34*, L18803, doi:10.1029/2007GL030168.
- Slingo, A., et al. (2006), Observations of the impact of a major Saharan dust storm on the atmospheric radiation balance, *Geophys. Res. Lett.*, *33*, L24817, doi:10.1029/2006GL027869.
- Sokolik, I. N., and O. B. Toon (1999), Incorporation of mineralogical composition into models of the radiative properties of mineral aerosol from UV to IR wavelengths, *J. Geophys. Res.*, *104*, 9423–9444, doi:10.1029/1998JD200048.
- Tegen, I., and I. Fung (1995), Contribution to the atmospheric mineral aerosol load from land surface modifications, *J. Geophys. Res.*, *100*, 18,707–18,726, doi:10.1029/95JD02051.
- Tegen, I., M. Werner, S. P. Harrison, and K. E. Kohfeld (2004), Relative importance of climate and land use in determining present and future global soil dust emission, *Geophys. Res. Lett.*, *31*, L05105, doi:10.1029/2003GL019216.
- Todd, M. C., R. Washington, M. Vanderlei, O. Dubovik, G. Lizzano, S. M'Bainayel, and S. Engelstaedter (2007), Mineral dust emission from the Bodélé Depression, northern Chad, during BoDEX 2005, *J. Geophys. Res.*, *112*, D06207, doi:10.1029/2006JD007170.
- Washington, R., and M. C. Todd (2005), Atmospheric controls on mineral dust emission from the Bodélé Depression, Chad: The role of the low level jet, *Geophys. Res. Lett.*, *32*, L17701, doi:10.1029/2005GL023597.
- Washington, R., M. Todd, N. J. Middleton, and A. S. Goudie (2003), Dust-storm source areas determined by the Total Ozone Monitoring Spectrometer and surface observations, *Ann. Assoc. Am. Geogr.*, *93*, 297–313, doi:10.1111/1467-8306.9302003.
- Webster, H. N., E. B. Carroll, A. R. Jones, A. J. Manning, and D. J. Thomson (2007), The Buncefield oil depot incident: A discussion of the meteorology, *Weather*, *62*(12), 325–330, doi:10.1002/wea.164.
- Witham, C., and A. Manning (2007), Impacts of Russian biomass burning on UK air quality, *Atmos. Environ.*, *41*(37), 8075–8090, doi:10.1016/j.atmosenv.2007.06.058.
- Woodward, S. (2001), Modeling the atmospheric life cycle and radiative impact of Mineral dust in the Hadley Centre Climate Model, *J. Geophys. Res.*, *106*(D16), 18,155–18,166, doi:10.1029/2000JD900795.
- Yoshioka, M., N. Mahowald, J.-L. Dufresne, and C. Luo (2005), Simulation of absorbing aerosol indices for African dust, *J. Geophys. Res.*, *110*, D18S17, doi:10.1029/2004JD005276.
- Zhu, A., V. Ramanathan, F. Li, and D. Kim (2007), Dust plumes over the Pacific, Indian, and Atlantic oceans: Climatology and radiative impact, *J. Geophys. Res.*, *112*, D16208, doi:10.1029/2007JD008427.

B. Anderson and G. Chen, NASA Langley Research Center, Hampton, VA 23681, USA.

H. Coe, School of Earth, Atmosphere and Environmental Science, University of Manchester, Manchester M13 9PL, UK.

K. Desboeufs and P. Formenti, LISA, CNRS, Universités Paris 12 et Paris 7, 61 Avenue du Général de Gaulle, F-94010 Créteil, France.

M. A. J. Harrison and S. Osborne, Met Office, Exeter EX1 3PB, UK.

E. J. Highwood and C. L. McConnell, Department of Meteorology, University of Reading, Reading RG6 6BB, UK. (c.l.mcconnell@reading.ac.uk)

S. Nava, National Institute of Nuclear Physics, I-50019 Florence, Italy.